Development and Investigation of GridRad-Severe, a Multi-Year Severe Event Radar Dataset

Amanda M. Murphy,[a] Cameron R. Homeyer,[a] and Kiley Q. Allen[a]

[a] *School of Meteorology, University of Oklahoma, Norman, OK, USA*

Corresponding author: Amanda M. Murphy, amanda.murphy@ou.edu

Early Online Release: This preliminary version has been accepted for publication in *Monthly Weather Review*, may be fully cited, and has been assigned DOI 10.1175/MWR-D-23-0017.1. The final typeset copyedited article will replace the EOR at the above DOI when it is published.

ABSTRACT: Many studies have aimed to identify novel storm characteristics that are indicative of current or future severe weather potential using a combination of ground-based radar observations and severe reports. However, this is often done on a small scale using limited case studies on the order of tens to hundreds of storms due to how time-intensive this process is. Herein, we introduce the GridRad-Severe dataset, a database including ~100 severe weather days per year and upwards of 1.3 million objectively tracked storms from 2010-2019. Composite radar volumes spanning objectively determined, report-centered domains are created for each selected day using the GridRad compositing technique, with dates objectively determined using report thresholds defined to capture the highest-end severe weather days from each year, evenly distributed across all severe report types (tornadoes, severe hail, and severe wind). Spatiotemporal domain bounds for each event are objectively determined to encompass both the majority of reports as well as the time of convection initiation. Severe weather reports are matched to storms that are objectively tracked using the radar data, so the evolution of the storm cells and their severe weather production can be evaluated. Herein, we apply storm mode (single cell, multicell, or mesoscale convective system) and right-moving supercell classification techniques to the dataset, and revisit various questions about severe storms and their bulk characteristics posed and evaluated in past work. Additional applications of this dataset are reviewed for possible future studies.

Accepted for publication in *Monthly Weather Review*. DOI 10.1175/MWR-D-23-0017.1.

1. Introduction

Severe weather, including tornadoes, severe hail, and severe wind, has substantial impacts across the U.S. each year. NCEI (2023) reported that severe weather accounted for approximately 8.5 billion dollars (inflation adjusted) in annual losses and nearly 2,000 deaths from 1980-2022. Additionally, there have been 163 severe weather events each totaling 1 billion dollars (inflation adjusted) in losses or more, including derechos, hail storms, and tornado outbreaks, and 38 events with 10 or more casualties over that same period. It remains important to analyze these, and other such high-end severe weather events, to further improve our resilience to them.

Examining a severe weather event is inherently multifaceted, and the data used depend primarily on the type of analysis. These data often include synoptic-scale and mesoscale data starting in the days to hours preceding an event (e.g., Rockwood and Maddox 1988; Coniglio et al. 2011; Hurlbut and Cohen 2014; Vaughan et al. 2017), radar and satellite data to examine storm-scale features and evolution during the event, and storm reports in the aftermath to evaluate impacts. Radar data can be incredibly useful to understand the physical and kinematic structure of severe vs. non-severe storms. In particular, such data have provided insight into the intensity of precipitation, horizontal and vertical extents, wind speeds, flow patterns, rotational velocities, and precipitation distributions associated with a storm (e.g., Byers and Braham 1949; Browning 1964; Brown et al. 1978; Lemon and Doswell 1979; Wurman et al. 1996; Parker and Johnson 2000). Radars have been used for several decades to understand tornadic storms and tornadogenesis (e.g., Lemon and Doswell 1979; Ryzhkov et al. 2002, 2005; Kumjian and Ryzhkov 2008; Kurdzo et al. 2017; Homeyer et al. 2020), estimate hail size in a storm (e.g., Witt et al. 1998; Murillo and Homeyer 2019), and better understand severe straight-line wind events (e.g., Fujita and Byers 1977; Fujita 1990; Wakimoto 2001; Klimowski et al. 2003). With the advent of dual-polarization radar and integration of such radars into the operational network of S-band radars in the U.S. (NEXRAD network) in 2013, a wealth of additional information can be inferred from these data including improved hydrometeor classification, detecting the presence and size of hail, convective updraft and vertical wind shear identification, and detection of tornadic debris (Kumjian 2013). Radar datasets therefore remain powerful tools to further understand the structure of severe storms and any unique identifying characteristics that can be used in real-time for warning decisions.

Accepted for publication in *Monthly Weather Review*. DOI 10.1175/MWR-D-23-0017.1.

One such radar analysis technique that has been performed both manually and objectively is storm mode classification. Accurate identification of storm mode allows for further insight into the potential for various types of severe weather. Common storm classifications include single cell storms, multicellular storms, and mesoscale convective systems (MCSs). For smaller-scale studies, subjective (manual) identification is often performed, as it is not prohibitively time intensive for so few samples. However, for studies using larger databases of storms, objective methods are a practical and often necessary solution for classification. Various studies use observed or simulated column-maximum reflectivity and a 30-40 dBZ threshold (e.g., Trapp et al. 2005; Snively and Gallus 2014; Thielen and Gallus 2019) to define contours encapsulating convective elements. Using radar data analyzed on the order of minutes to hours, these techniques often incorporate constraints for aspect ratio (i.e., the length to width ratio; e.g., Bluestein and Jain 1985; Fowle and Roebber 2003; Gallus et al. 2008; Smith et al. 2012; Snively and Gallus 2014; Thielen and Gallus 2019), maximum contour dimension (e.g., Bluestein and Jain 1985; Parker and Johnson 2000; Trapp et al. 2005; Gallus et al. 2008; Smith et al. 2012; Snively and Gallus 2014; Thielen and Gallus 2019), enclosed area (e.g., Fowle and Roebber 2003), and storm persistence/duration (e.g., Geerts 1998; Pinto et al. 2015; Feng et al. 2018, 2019).

Beyond determining a storm's mode, one common approach to analyzing their severe weather potential is through case studies, especially using radar observations and severe reports. Case studies of severe weather events and their radar presentations abound in the literature, providing valuable fine-scale insight into the inner workings of severe thunderstorms. For example, a case study examination of a tornadic supercell in Oklahoma on 3 May 1999 led to the discovery of the polarimetric radar tornadic debris signature (TDS) by Ryzhkov et al. (2002), prompting analyses of other supercells for potential analogous signatures in Ryzhkov et al. (2005) and the eventual inclusion of the polarimetric TDS in modern guides on polarimetric radar utility (e.g., Kumjian 2013). Additionally, Fujita and Byers (1977) examined the meteorological conditions surrounding an airplane crash and detected thunderstorm winds that were much stronger than anything previously observed, coining these winds a "downburst." This observation prompted numerous field campaigns targeting downburst-producing storms (e.g., Fujita and Wakimoto 1982; McCarthy et al. 1982; Wilson et al. 1988), leading to a more comprehensive understanding of the phenomenon today and likely saving many lives (Wilson and Wakimoto 2001). Working with case

Accepted for publication in *Monthly Weather Review*. DOI 10.1175/MWR-D-23-0017.1.

studies allows for very detailed analyses of severe storms, but the conclusions from such studies are limited in generalizability given their relatively small sample sizes.

Large-scale studies of severe weather in the literature date as far back as the 1940s with the Thunderstorm Project (Byers and Braham 1949), and climatological studies have driven many of the scientific community's advances in severe weather knowledge. Tornadoes in the U.S. are most common in early summer (Brooks et al. 2003) and in the late afternoon to early evening (Ashley et al. 2008), mostly in the Great Plains and into the Southeast (Coleman and Dixon 2014; Gensini and Brooks 2018; Krocak and Brooks 2018). The majority of reported tornadoes are weak (EF-0 to EF-1; e.g., Brooks and Doswell 2001; Trapp et al. 2005) although the less frequent significant tornadoes (EF 2+) are responsible for nearly 90% of fatalities (e.g., Anderson-Frey and Brooks 2019). Climatologies of severe hail like those by Cintineo et al. (2012), Murillo et al. (2021), and Wendt and Jirak (2021) are also typically built using reports, despite well-known reporting limitations (see Allen and Tippett 2015, and references therein). Allen and Tippett (2015) examined a 60-year record of over 260,000 hail reports and found that the majority of all hail reports occurred in the late afternoon to early evening primarily during the late spring, with a maximum in the Great Plains that is slowly shifting northward. Studies of severe winds often focus attention on MCSs, which can produce uniquely widespread and damaging severe winds, including and especially from derechos (Johns and Hirt 1987; Corfidi et al. 2016). Coniglio and Stensrud (2004) found that higher-end derecho events in their 16-year climatology favor the southern plains and Midwest. Derechos in the eastern two-thirds of the CONUS tend to occur more in the summer months (Coniglio and Stensrud 2004) in the late evening to overnight (Bentley and Mote 1998). Recent work using machine learning to classify and track MCSs and quasi-linear convective systems (QLCSs) by Ashley et al. (2019) showed, using their developed MCS climatology, that nearly a third of all MCSs in their 22-year dataset were also QLCSs, and QLCS storms were linked with 28% of all severe wind reports in the central and eastern U.S. Climatological studies allow for a large-scale view of severe weather to develop mental models for how, when, and where severe hazards are likely to occur.

Several studies have investigated compelling scientific questions about severe storms beyond just their climatological distributions using a large record of observations. For example, studies such as Homeyer et al. (2020), Loeffler et al. (2020), and Van Den Broeke (2020) use radar data from tens

Accepted for publication in *Monthly Weather Review*. DOI 10.1175/MWR-D-23-0017.1.

to hundreds of tornadic and nontornadic supercells to examine tornadogenesis predictability; Blair et al. (2011) and Gutierrez and Kumjian (2021) examined radar signatures within tens to hundreds of giant and gargantuan hail-producing storms; and Bluestein and Jain (1985) and Schiesser et al. (1995) looked at mesoscale structures within radar data from dozens of severe MCSs. Past studies such as these, despite using larger datasets than the more numerous case study analyses, rarely contain more than a few hundred storms and are commonly limited in both their spatiotemporal extent and temporal resolution of observations. Furthermore, any larger-scale studies done before 2013 have limited to no access to polarimetric radar data, which further limits understanding of storm microphysics that may be relevant to severe events. Therefore, there exists a need to expand these studies using a longer temporal record and analyze a much larger population of storms that are more spatiotemporally diverse, have higher temporal resolution data, and that occurred within the observational range of one or more polarimetric radars.

Recognizing the contributions of the aforementioned prior work to our understanding of severe storms, and with the increasing record of observations and emergence of a national polarimetric radar network, a clear incentive exists to create a modern database of radar data and severe weather reports to evaluate the characteristics of storms that produce severe weather. This paper aims to fill the knowledge gaps outlined herein using the newly developed GridRad-Severe database (hereafter abbreviated GR-S): a database including gridded multi-radar data covering the majority of the CONUS, objective storm tracks, and storm reports. Herein, we outline the creation and utility of GR-S as well as how well it reflects the spatiotemporal distribution of all storm reports in the U.S. Additionally, we introduce objective storm mode and supercell classification techniques to aid in data analysis, and examine initial findings of the GR-S dataset that complement and expand upon past studies. Finally, we directly compare GR-S findings with results from select seminal papers to demonstrate its ability to replicate and extend prior key findings.

2. The GR-S dataset

a. Radar data

Radar data sourced from the nationwide NEXRAD network (NOAA/NWS/ROC 1991; Crum and Alberty 1993) were used to create GridRad data using version 4.2 of the public algorithm (Homeyer and Bowman 2022). GridRad data are merged volumes of individual radar observations across

Accepted for publication in *Monthly Weather Review*. DOI 10.1175/MWR-D-23-0017.1.

the CONUS, binned on a regular longitude-latitude grid. This includes single-polarization radar moments such as radar reflectivity at horizontal polarization (Z_{H}) and radial velocity spectrum width (σ_V) before 2013, and additional dual-polarization variables such as differential radar reflectivity (Z_{DR}), co-polar correlation coefficient (ρ_{hv}), and specific differential phase (K_{DP}) following the polarimetric upgrade of the radar network. Derived kinematic variables were also calculated on the native grid of each radar and binned into GridRad volumes and include radial divergence and azimuthal shear of the radial velocity. The spatial resolution of GridRad data is ~0.02 × ~0.02 degrees longitude-latitude (48 grid points per degree), and 0.5-km vertical resolution up to 7 km above mean sea level (AMSL), after which the vertical resolution coarsens to 1-km up to 22 km AMSL. Temporal resolution of the data is 5 minutes. More technical details about the creation of GridRad data can be found in Homeyer and Bowman (2022). GridRad is one of a few commonly used merged CONUS radar products (notable alternatives include NOAA's Multi-Radar Multi-Sensor [MRMS] and Multi-Year Reanalysis of Remotely Sensed Storms [MYRORSS]) and is unique in its breadth of merged radar variables and merging methods that aim to provide high-fidelity echo top heights and internal storm structure. Herein, we only create GridRad data for severe events within the CONUS (specifically, domains spanning 24 to 50° N and 125 to 66° W).

The GR-S database includes radar data from 2010-2019 inclusive, with future years expected to be added over time. This dataset starts in 2010 due to both good NEXRAD coverage and being after the NEXRAD transition to super resolution (Torres and Curtis 2007). Since the tornado rating scale changed from F to EF in 2007 (Doswell et al. 2009; Edwards et al. 2013) and the severe hail size threshold changed from 0.75" to 1.0" in early 2010 (before the first date in this dataset; Allen and Tippett 2015), all reports classified as severe herein are based on a uniform threshold for hail (≥ 1.0") and wind (gusts ≥ 50 kts) and a uniform damage rating scale for tornadoes (the Enhanced Fujita or EF scale). Significant severe reports are those meeting or exceeding EF-2 for tornadoes, 2.0" for hail, and 65 kt gusts for wind (Hales Jr. 1988).

b. Storm report data

Storm report data are sourced from NOAA's Storm Events Database (SED) hosted at the National Centers for Environmental Information (NCEI/NOAA 2022) from 2010 through 2019 inclusive, including tornado, hail, and wind report data. Each SED report includes a unique event ID, start

Accepted for publication in *Monthly Weather Review*. DOI 10.1175/MWR-D-23-0017.1.

and end date and time, initial and final event coordinates (longitudes and latitudes), and magnitude (EF rating for tornadoes, maximum diameter for hail, and maximum wind speed for severe wind). Tornado reports also include tornado path length and width.

c. Event definition

Defining a GR-S event occurs in a few distinct steps. First, high-end severe days are identified using the tornado, hail, and wind reports from the SED. To be consistent with SPC severe days and most prior work, GR-S events begin at 12 UTC on the event day and end at 12 UTC on the following day. We identify days as high-end severe days if the number of tornado, hail, or wind reports exceeds 8, 45, or 120, respectively. These primary thresholds were chosen because they result in a nearly balanced dataset of high-end tornado, hail, and wind days each year, with approximately 100 days per year being labeled as high-end severe days (i.e., GR-S events). The thresholds also approximately correspond to the 85th percentile of daily report counts for each hazard. Once a day is included in the GR-S database (via the aforementioned primary threshold), secondary thresholds are used to determine what severe types will be used for domain definition on that day, roughly corresponding to the upper quartile of daily report counts. This is done to maximize the diversity and breadth of severe weather that is analyzed on the selected GR-S event days; if a day is already included in the dataset, it makes sense to analyze not only the severe hazard that happened enough times to warrant the day's inclusion in the dataset, but also any other severe hazards that, while not prolific enough to pass that high primary threshold, still frequently occurred on that day. The secondary thresholds are roughly one-half of the primary thresholds: greater than 4 tornado reports, 22 hail reports, or 60 wind reports. Isolating data in these ways results in a large dataset focused solely on high-end severe weather events with a high level of spatiotemporal detail.

After high-end severe days are identified, the locations and times of the SED reports are used to constrain the spatiotemporal domains of each day's GridRad data. Domain bounds are objectively determined using the latitudes, longitudes, and times of reports for each day's selected report types (i.e., tornado, hail, and/or wind). These space and time bounds are independently created for each report type and the final domain results from retaining the extrema of each objective report domain. First, the mean latitude and longitude to the nearest half degree of a given report type is found. An initial box encompassing this point is created with bounds ± 5 degrees longitude and latitude

Accepted for publication in *Monthly Weather Review*. DOI 10.1175/MWR-D-23-0017.1.

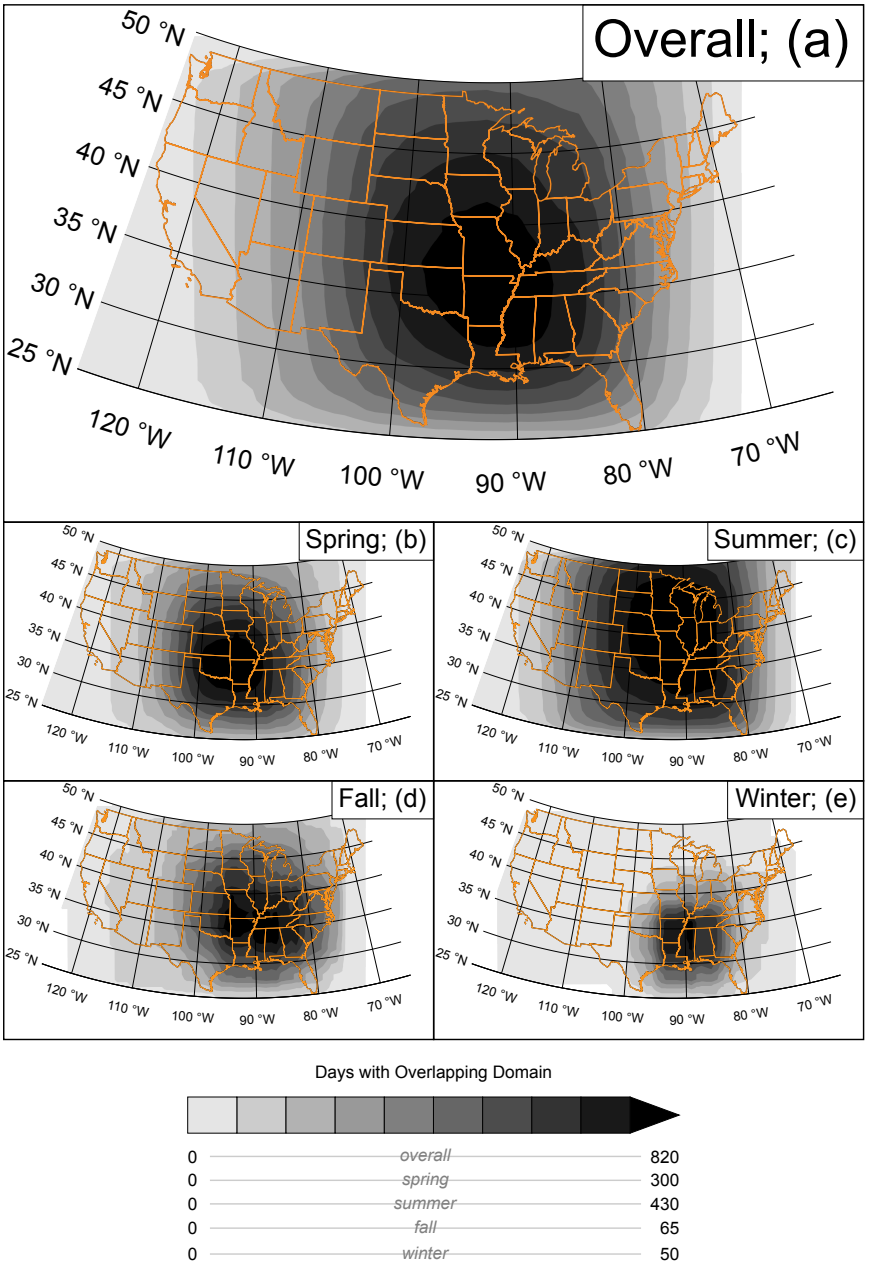

FIG. 1. Contour plots of the number of times a point was encompassed within a GR-S domain, gridded to an approximate 80 × 80 km grid. Plots include (a) all GR-S days; (b) days in March, April, and May (spring); (c) days in June, July, and August (summer); (d) days in September, October, and November (fall); and (e) days in December, January, and February (winter). Colorbar limits are individual to each panel, and listed below the colorbar at the bottom. State borders are highlighted in orange.

Accepted for publication in *Monthly Weather Review*. DOI 10.1175/MWR-D-23-0017.1.

from the mean report location. This 10° × 10° box then recursively expands by 0.5 degrees in all directions until ≥ 90% of reports for that report type are encompassed. Using only those reports enclosed in the objectively identified box, time boundaries are created in a similar manner, starting with ± 2 hours centered on the mean report time rounded to the nearest half-hour. The time boundaries expand recursively by half-hour increments in each direction until ≥ 90% of the reports within the spatial boundaries are captured (i.e., ≥ 81% of the total number of reports). Note that the time bounds of a GR-S event (1200-1200 UTC) differ slightly from the SPC definition of a single day (1200-1159 UTC). Once these time boundaries are determined, they are trimmed such that the start time is no more than 30 minutes before the first report and the end time is no more than 30 minutes after the last report. This ensures that the GridRad data created are focused on the times when severe weather was occurring. Figure 1 shows how often a location was encompassed within a GR-S domain. Overall, the GR-S domains were generally focused on the region from 100°-80° W and 30°-45° N, offset slightly southeast of the center of the CONUS. As the year cycles from spring through winter, the GR-S domains on average shift in a clockwise manner, consistent with seasonality in the SED report data (not shown).

As stated previously, this creation of space and time bounds is done independently and objectively for each report type that exceeds its secondary threshold. For days where more than one report type exceeds its secondary threshold, both a composite spatial domain and a composite temporal domain are created using the individual spatial and temporal domains for each report type, retaining the overall maximum and minimum latitudes, longitudes, and times to create a composite domain that encompasses all individual domains. Once these spatiotemporal bounds are determined, the time bounds are limited to begin no earlier than 15 UTC on the event day and end no later than 12 UTC the following day, to limit analyses to the 12 UTC-12 UTC period used for SED reports. We use 15 UTC instead of 12 UTC as the start time limit because all GR-S day temporal domains are then extended backward by 3 hours to attempt to capture convection initiation (CI). This is motivated by prior work such as Bluestein and Parker (1993), which found in their dryline study in Oklahoma that the time between CI and the first tornado report for a storm was approximately 2-3 hours (see their Table 2). A flowchart describing these methods is shown in Fig. 2, and an additional schematic showing an example GR-S case and spatiotemporal domain selection is available as supplemental material.

Accepted for publication in *Monthly Weather Review*. DOI 10.1175/MWR-D-23-0017.1.

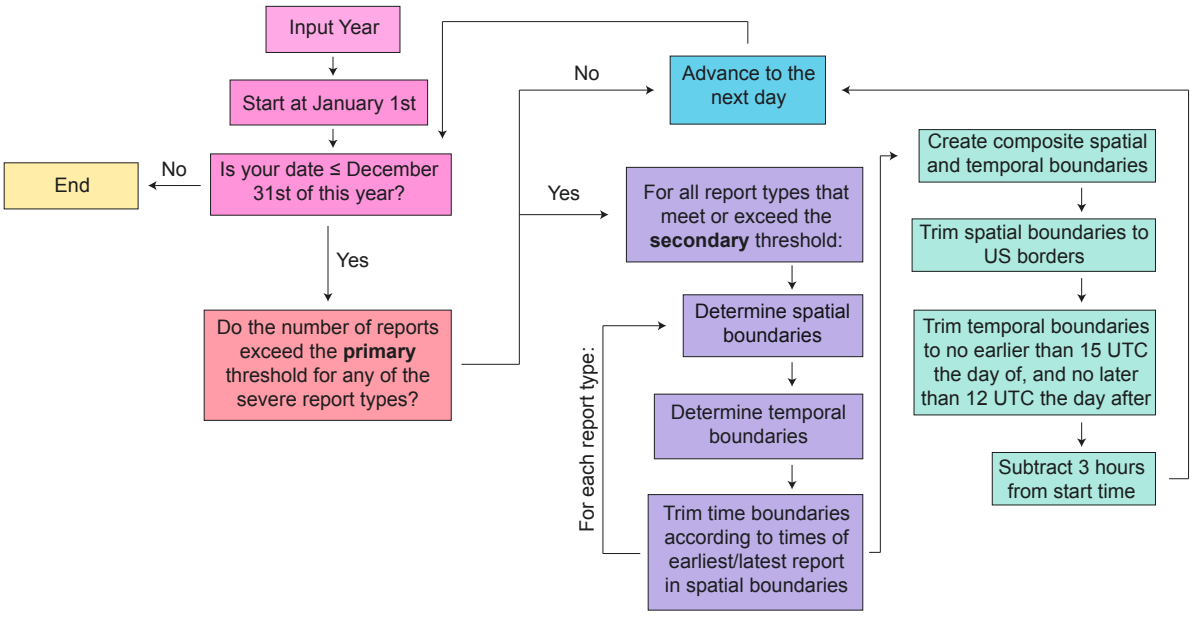

FIG. 2. Flowchart explaining the creation of GR-S data for a given year.

d. GR-S storm tracks

Each GR-S event includes the 5-min GridRad volumes outlined in section 2a and a comma-delimited storm track file that includes official storm reports matched with each storm. The storm tracks for each event are identified using an echo-top altitude-based tracking method from Homeyer et al. (2017), with modification to resolve premature termination of tracks during storm splits and mergers as outlined in Lagerquist et al. (2020). In summary, the GridRad storm tracking algorithm identifies point locations of Z_H = 30-dBZ echo-top altitude maxima and links them in time (5-min intervals for GR-S). Echo-top maxima are required to reach at least 4 km AMSL and be embedded within echoes classified as convection by the Storm Labeling in 3 Dimensions algorithm (SL3D; Starzec et al. 2017) to be tracked. Cells in subsequent time steps are linked in time if they are located within 15 km of each other (for neighboring 5-min volumes only). In cases where more than one echo-top maximum is located within 15 km of a previously defined storm, the closest one is matched during tracking. Finally, the tracking algorithm only retains tracks that are at least 15 minutes in duration–or, equivalently, are identified in at least three consecutive 5-minute GridRad volumes. To resolve storm splits and storm mergers, colinear storm tracks with closely located or overlapping initial and final locations and times are combined into one track. This combination

Accepted for publication in *Monthly Weather Review*. DOI 10.1175/MWR-D-23-0017.1.

ensures that cyclic updraft cycles, as seen commonly in supercells, are not split into multiple short-duration storm tracks. Two passes are made in this attempt to combine broken storm tracks: i) joining tracks with end and start times separated by one 5-min GridRad analysis (gap storms) so long as their end and start locations differ by $\leq$ 15 km, and ii) joining storms with start and end times that fall within one 5-min GridRad analysis of each other, so long as the minimum distance between track locations during the overlapping period is $\leq$ 15 km. In the former, the location during the gap is determined using linear interpolation between the end and start locations of the combined tracks. In the latter, tracks are combined at the closest point of coincidence during overlap such that the point of the second (later) track through its remaining path is appended to the first (earlier) track. An illustration of the various track combination cases is included as supplemental material.

After the initial storm tracking and track combination algorithms are applied to each GR-S event, the resulting 5-minute storm tracks are linearly interpolated to 1-minute resolution for spatiotemporal collocation with SED reports. To match the SED reports to the storm tracks, the closest tracked storm to a report at the report time is matched, so long as it lies within 30 km of the report location. While a maximal 30-km radius for report matching may be considered generous, it is noted that nearly all matched reports fall within 10-15 km of the objectively tracked storm centers and manual validation efforts in the past have demonstrated broad reliability of this approach (e.g., Homeyer et al. 2020). Figure 3 shows how storm reports are matched to storm tracks for the 14 April 2011 GR-S event. Matching reports with storm tracks in this way allows for individual storms to be classified as sub-severe or severe, and their individual characteristics examined in a bulk sense. An important limitation to accurate report matching is the spatiotemporal accuracy of the reports themselves; many studies (e.g., Trapp et al. 2006; Allen and Tippett 2015, for severe wind and hail reports, respectively) have reported on the imperfect nature of human-reported severe weather. These limitations are an important consideration in any work using storm reports as a method of validation.

The final archived 1-minute, comma-delimited storm track files contain information on storm location, motion, radar characteristics, and storm-matched severe reports (summarized in Table 1). In the case of severe hail or wind reports, the event information is linked to the midpoint time of the report so that no report gets counted more than once. For tornado reports, most of the report information is linked to the initial report time (i.e., tornadogenesis).

Accepted for publication in *Monthly Weather Review*. DOI 10.1175/MWR-D-23-0017.1.

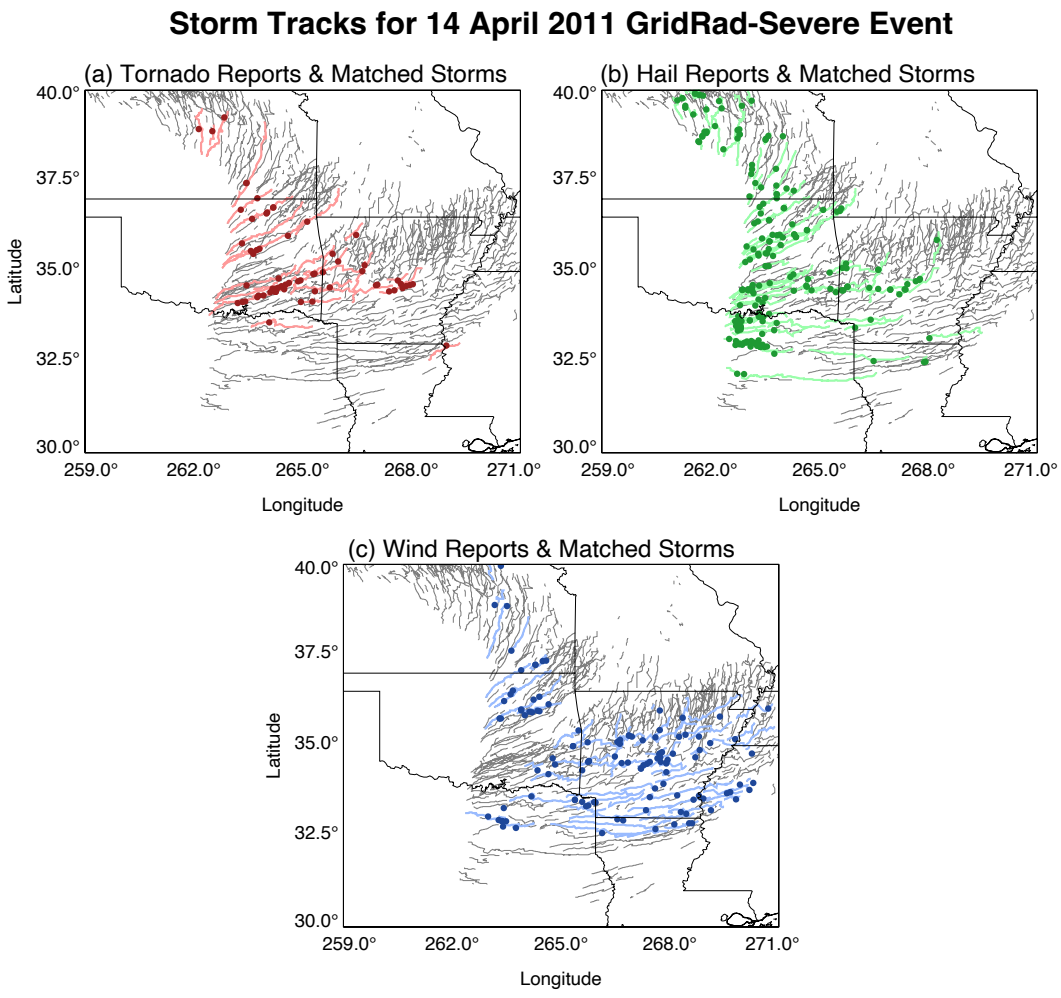

FIG. 3. GR-S storm tracks for the 14 April 2011 event, with severe reports superimposed as dark circles and storm tracks matched with reports in a lighter shade of the same color for (a) tornadoes, (b) hail, and (c) wind. Storm tracks not matched with a report are shown in gray.

While enabling unique analyses of the GR-S data, limitations to the objective storm tracking methods do exist. Common drawbacks include unresolved storm splits and mergers and poorly tracked initiation phases of some storms (before $Z_H = 30$ dBZ exists and/or before the 30-dBZ echo top exceeds 4 km AMSL, which is typically <15 minutes in severe storms).

Accepted for publication in *Monthly Weather Review*. DOI 10.1175/MWR-D-23-0017.1.

Information in GR-S Event Storm Track Files	
Storm Information	Report Information*
Storm Number	Binary Report Flag
Storm Date & Time	Report Number
Storm Longitude	Report Longitude
Storm Latitude	Report Latitude
Eastward Storm Motion	Report Magnitude
Northward Storm Motion	Instantaneous Tornado Count
Echo Top Altitudes	Max Instantaneous Tornado Rating
Column-Maximum Z_H	Tornado End Date & Time
	Tornado Width
	Tornado Length

TABLE 1. Storm attributes included in GR-S event track files, separated for radar-based storm information (left column) and matched SED report information (right column). *Report flag (0 or 1), number, longitude, latitude, and magnitude are given for all report types (tornado, hail, and wind), where for tornadoes the report information is listed only at the time of tornadogenesis. The additional SED report information for tornado end time, width, and length are also only given at the time of tornadogenesis, while the instantaneous tornado count and maximum rating are based on all reports valid at each 1-min storm track time.

3. Analysis methods

a. Storm mode classification

Given that many past studies have classified storm mode subjectively, such efforts have often focused on small spatiotemporal domains. An objective method for storm mode classification is presented herein for use with the GR-S dataset. This storm mode classification relies on closed radar echo contours above a given Z_H threshold encompassing objectively tracked storms to be able to classify each track within a contour as a part of a single cell storm, multicell storm, or an MCS. By classifying the mode of each objectively tracked storm, characteristics of each storm can be analyzed in concert with storm-matched SED reports to potentially link storm mode and storm-scale characteristics with the presence of (or lack thereof) severe weather.

To classify storm mode, 30-dBZ contours are identified using column-maximum reflectivity (Z_{Hmax}) from each 5-min GridRad data file. For each closed contour, the area and maximum dimension are calculated, and the number of tracked storms within each contour is counted. Tracked storms are then identified as single (i.e., discrete) cell if either 1) only a single tracked storm exists within a contour, or 2) a relatively small contour (< 3000 km^2) encompasses no more

Accepted for publication in *Monthly Weather Review*. DOI 10.1175/MWR-D-23-0017.1.

than two tracked storms. Two tracked storms within a small contour are both classified as single cell to account for storms with cyclic updraft generation (e.g., supercells) that can have more than one updraft at a single time, but do not persist as such. Homeyer et al. (2020) found in their composite analyses of supercells that the average supercell size for Z_{Hmax} = 30 dBZ is approximately 3000 km^2 (their Fig. 3). The 3000 km^2 contour area threshold is therefore chosen to encompass the size of some of the largest single cell storms expected. For larger contours ($\geq$ 3000 km^2) containing 2 tracked storms or any contour containing 3 or more tracked storms, those storms are classified as either multicell or MCS. The delineation between the two is made using the contour maximum dimension; if the maximum dimension is $\geq$ 100 km, it is classified as an MCS (Houze Jr. 2004).

Since the storm mode classification algorithm is independently run on each time step, a tracked storm may have a complex, time-varying storm mode classification. We do not employ a minimum time that a tracked storm has to be identified as a consistent storm mode to retain such a classification. This is done because, instead of classifying a storm based on its mean storm mode, we want to enable investigation into how each storm evolves in time and, if possible, how changes in its severity accompany changes in storm mode. Figure 4 shows select times during the evolution of the 14 April 2011 GR-S event in the southern plains. Over time, many single cell storms that initiated early in the event merge into what eventually becomes a large MCS. In concert with matched storm reports (e.g., Fig. 3), storm mode can be linked with a storm's severity for bulk analyses of the two characteristics.

Accepted for publication in *Monthly Weather Review*. DOI 10.1175/MWR-D-23-0017.1.

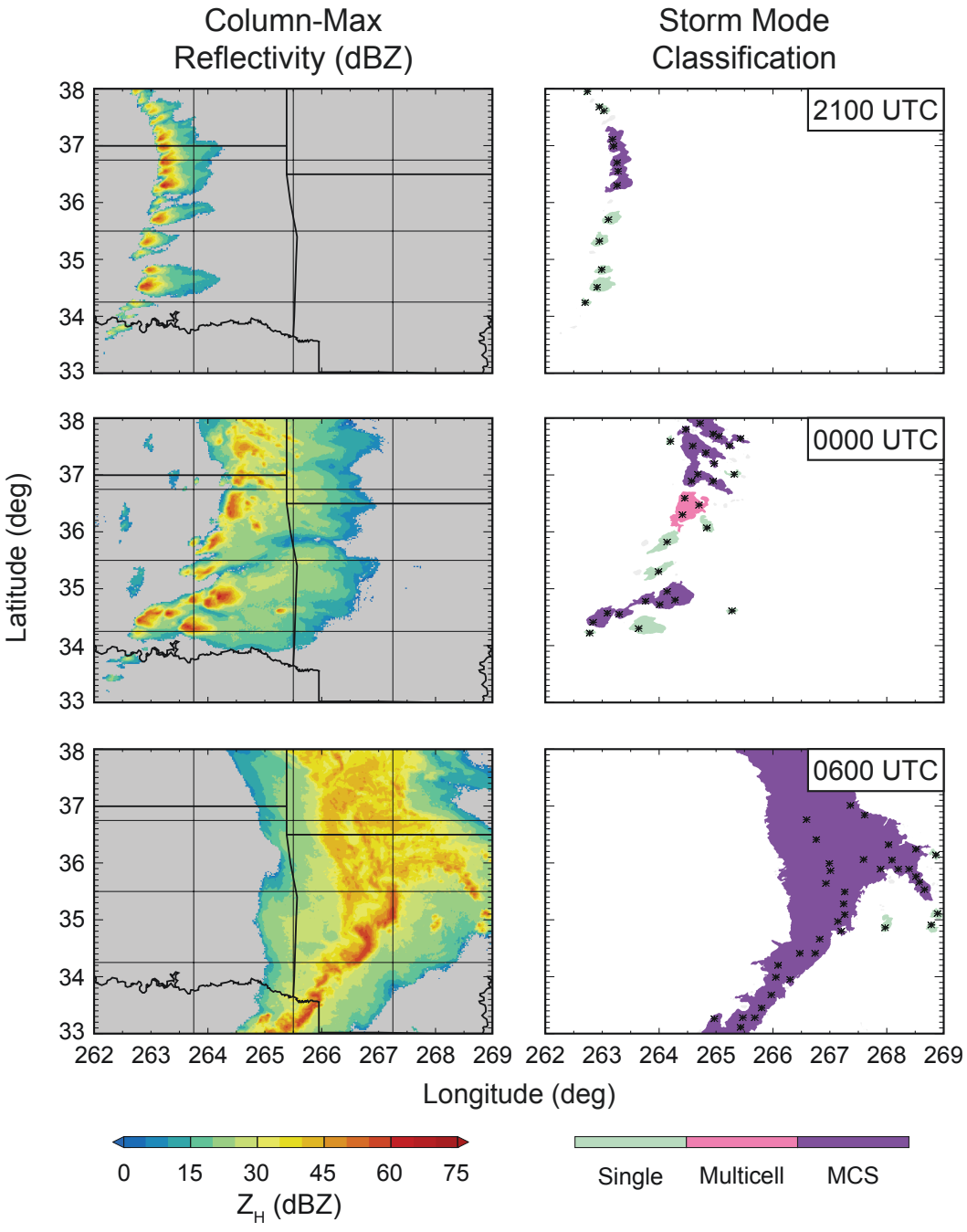

FIG. 4. Select images of (left) column-max reflectivity and (right) storm mode classification from a limited spatial domain within the 14-15 April 2011 GR-S case. For storm mode classification images, the interior of identified 30-dBZ contours are shaded in green, pink, or purple to denote single cell, multicell, or MCS classification, respectively. Tracked storms within such contours are indicated by black asterisks. Identified 30-dBZ contours that do not encompass any storm tracks are shaded in light gray.

Accepted for publication in *Monthly Weather Review*. DOI 10.1175/MWR-D-23-0017.1.

b. Mesocyclonic updraft classification

Another important severe storm characteristic is whether or not a storm's updraft was rotating when the storm produced a severe report. Updrafts that have sufficient persistent rotation are defined herein as mesocyclonic, and otherwise as non-mesocyclonic. Mesocyclonic updrafts are classified using the methods for right-moving supercell identification outlined in Homeyer et al. (2020), originally based on work by Sandmæl (2017). Namely, five criteria are used to objectively identify updrafts as mesocyclonic: 1) maximum midlevel (4-7 km AMSL) azimuthal shear exceeds $4 * 10^{-3}$ s^{-1} for at least 40 minutes; 2) maximum midlevel azimuthal shear meets or exceeds $5 * 10^{-3}$ s^{-1}; 3) maximum column-max azimuthal shear meets or exceeds $7 * 10^{-3}$ s^{-1}; 4) maximum column-max radial divergence meets or exceeds $1 * 10^{-2}$ s^{-1}; and 5) maximum column-max velocity spectrum width meets or exceeds 13 m s^{-1}. The sixth criterion used in Homeyer et al. (2020)–max 40-dBZ echo top altitude meets or exceeds 11 km–was not applied in this study. This was done to enable reliable classification of wintertime convection, which often has lower echo tops.

It is important to note that the mesocyclonic updraft classification criteria were based on right-moving supercell identification criteria, so left-moving (mesoanticyclonic) storms are not independently examined herein. Both anecdotal evidence and prior research show a dearth of left-moving supercells compared to right-movers. Bunkers et al. (2006) examined long-lived supercells and found that, of 184 long-lived supercells in their dataset, only 4 were left-movers. An approximate ratio of left- to right-moving supercells is, to our knowledge, unknown. Future work may focus on classification of left-moving supercells using GR-S or an alternative dataset and further investigation of their characteristics compared to right-movers.

The result of these classification techniques is that each individual tracked storm has a time-varying storm mode classification and a binary mesocyclonic updraft classification. This can, and does, result in classifications such as multicell or MCS storms with mesocyclonic updrafts. Examples of these types of storms may include supercells that share the same 30-dBZ precipitation shield, mergers of a discrete supercell with a QLCS, supercells present in the early organizing stages of a QLCS (e.g., Weisman and Trapp 2003) or generation of vortices that meet mesocylonic rotation criteria (e.g., DeWald and Funk 2002). The identification of multicells and storms within MCSs that meet mesocyclonic updraft criteria in GR-S data allow for filtering of these storms if desired. Herein, these storms and their attendant severe weather are retained and examined in

Accepted for publication in *Monthly Weather Review*. DOI 10.1175/MWR-D-23-0017.1.

Section 4, but are removed in Section 5 where GR-S MCS storms that produced severe weather are compared to objectively identified severe MCSs and QLCSs.

4. Results

In order for conclusions in this study to be representative of the total climatology of severe weather and therefore broadly applicable, the distribution of GR-S storm matched reports must be representative of the complete SED database. Representativeness herein includes capturing not only the majority of SED reports, but also the correct spatiotemporal distribution. Looking at only the number of total SED reports vs. GR-S storm-matched reports, Table 2 summarizes the percent of severe and significant severe reports captured by GR-S for 2010-2019. Of all SED reports during those ten years, the GR-S data retains ~63–77% of total reports and ~68–91% of significant severe reports, with percent matched highest for tornado reports and lowest for wind reports. Focusing only on SED reports that existed within the spatiotemporal bounds of the GR-S domains, the range of retained reports increases to ~88–94% for all reports and ~91–98% for significant severe reports, again with percent matched highest for tornado reports and lowest for wind reports. This means that for all SED reports within the spatiotemporal bounds of the GR-S domains, the GR-S storm tracking and report matching procedure matches approximately 9 out of every 10 reports to a storm. Examining the total number of reports captured, the GR-S database retains 164748 out of the total 249600 SED reports during the 10-year period (~66%). This is expected since the GR-S database only includes ~100 days per year, with data only within limited spatiotemporal domains. However, it is encouraging that, if a report exists within a GR-S domain, it is highly likely that it will be matched with a GR-S tracked storm. Therefore, the domain selection criteria coupled with the matching algorithm are both capturing a majority of SED reports and effectively matching reports within GR-S bounds to objectively tracked storms.

Capturing the majority of severe reports is only one facet of examining the representativeness of the GR-S data. Equally important is the distribution of the reports–spatial and temporal, for both severe and significantly severe events–and whether those distributions match the full SED report climatology. Figure 5 shows the breakdown of total reports by month for both GR-S matched reports and SED reports, with lines showing the percent contribution of tornado/hail/wind reports to the total reports in each month. Tornado data in this figure and for all future analyses are focused

Accepted for publication in *Monthly Weather Review*. DOI 10.1175/MWR-D-23-0017.1.

Comparison of SED and GR-S Storm-Matched Reports			
Report Type	(1) % of SED Total	(2) % of SED within GR-S Bounds	(3) Total GR-S Reports
Tornado Initiations	76.83%	94.16%	10542
Hail Reports	70.60%	94.33%	56025
Wind Reports	62.72%	87.81%	98181
Sig. Tornado Initiations	90.85%	97.69%	1608
Sig. Hail Reports	79.85%	94.68%	5842
Sig. Wind Reports	67.80%	90.56%	7179

TABLE 2. Comparison of SED and GR-S matched reports from 2010-2019. For each tornado/hail/wind, data include (1) percent of GR-S matched reports compared to all SED reports of that type and over that period; (2) percent of GR-S matched reports compared to SED reports of that type and over that period, confined within the corresponding day's GR-S spatiotemporal bounds; and (3) the total GR-S matched reports in the dataset. Data are also shown isolating significant severe reports.

on the time of tornado initiation. The difference in total data points represented on each plot is captured by the y-axes, which show the mean 34% decrease in reports when comparing SED to GR-S data. The monthly distribution of reports is similar between the GR-S and SED data, although month-to-month variations in percent of SED reports captured within GR-S are visible. Percent differences between GR-S and SED reports per month range from 11-56%, with some of the lowest percent differences in the late spring and early summer (below 19% from April to June, inclusive). This is potentially due to a preference for higher-end severe days to occur in the spring to early summer, so a higher percentage of all severe weather days in that period would be captured by the GR-S domain selection criteria. Notably, April through June alone make up 51.8% of all GR-S days in this dataset. If only SED reports within the GR-S bounds are considered (not shown), those percent differences range from 8-28%, and are lowest in the spring and summer (8-11%) and highest in fall and winter (11-28%). Therefore, the storm tracking technique is most effective at tracking severe convection and matching reports to those storms during the maximum of the annual cycle in severe weather (the early-mid warm season) and least effective during the the cool season. Despite these differences, the GR-S bar graph still closely resembles the SED bar graph, showing that GR-S is capturing the overall distribution of severe reports quite well. The percent contribution of tornadoes, hail, and wind to each month's overall report count also show very similar values between the GR-S and SED data, demonstrating a monthly GR-S report type

Accepted for publication in *Monthly Weather Review*. DOI 10.1175/MWR-D-23-0017.1.

balance that is representative of the underlying SED report data. Overall, this analysis shows that the GR-S database captures the annual cycle of all SED reports well.

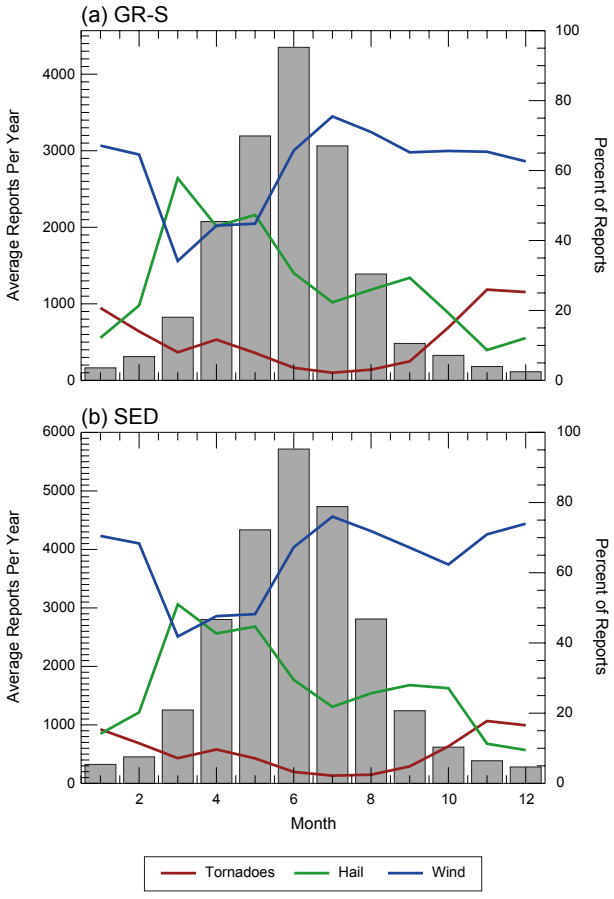

FIG. 5. Comparison of (a) GR-S and (b) SED average annual storm reports, broken down by month for 2010-2019. Lines indicate the percent contribution of various severe report types (tornado, hail, and wind) to the total number of reports in a given month. Pearson correlation coefficients comparing GR-S and SED lines for each severe hazard exceed 0.95.

Accepted for publication in *Monthly Weather Review*. DOI 10.1175/MWR-D-23-0017.1.

In addition to the annual cycle of reports, capturing the spatial distribution of reports is also very important. Figure 6 shows the gridded number of all SED reports from 2010-2019 for each severe report type juxtaposed with the gridded number of reports retained in the GR-S storm tracks. More reports are expected on the SED maps, again since GR-S events only include ~100 days per year of severe weather. Qualitatively, maps of GR-S matched reports and SED reports have similar spatial distributions, confirming that the distribution of reported severe weather is well captured in the GR-S database. In combination with Table 2, Fig. 6 gives confidence that GR-S is capturing the majority of reports in a consistent way across most of the CONUS. This can be more directly examined in Fig. 7, which shows both the total report difference between the GR-S database and the SED record and the percent difference between the two. These plots further demonstrate that reports are well matched across the eastern two-thirds of the country where reports are more frequent (Fig. 6). The areas with high percent differences are commonly found in locations with low report counts for both GR-S and SED (e.g., compare total number of reports in Fig. 6f to percent difference in Fig. 7f for severe wind in the western CONUS), meaning that while the percent of reports missed in these regions may be quite high, the total number of reports missed is quite low. Therefore, based on the results shown in Figs. 5–7, we can confidently say that the storm-matched reports within the GR-S database are a representative sample of the total climatology within the SED dataset.

Accepted for publication in *Monthly Weather Review*. DOI 10.1175/MWR-D-23-0017.1.

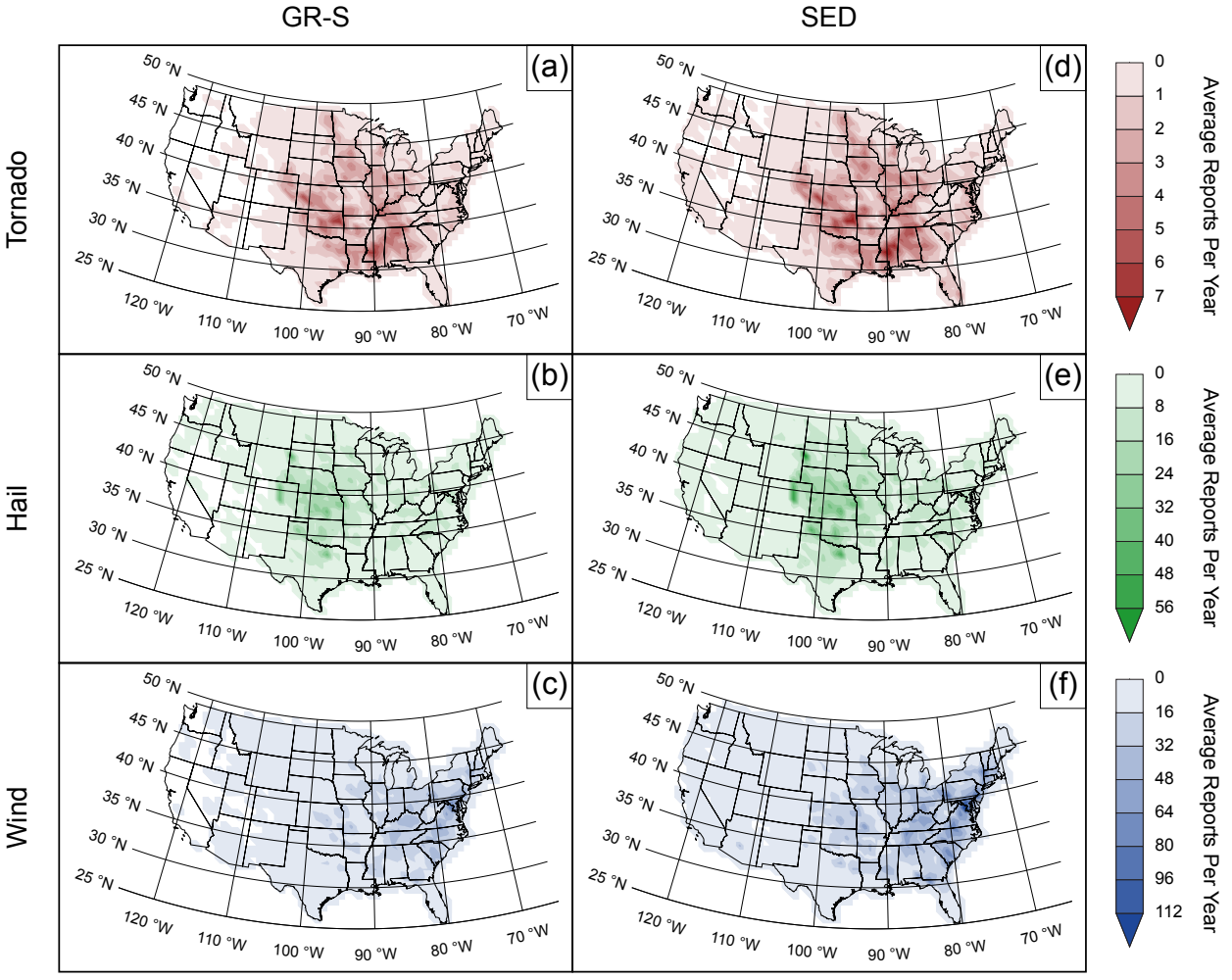

FIG. 6. Contour plots of average annual number of (a-c) GR-S and (d-f) SED reports for (a,d) tornado, (b,e) severe hail, and (c,f) severe wind reports from 2010-2019, inclusive. Data are gridded on an approximately 80 × 80 km grid. Areas not shaded indicate no (a-c) GR-S or (d-f) SED reports.

Accepted for publication in *Monthly Weather Review*. DOI 10.1175/MWR-D-23-0017.1.

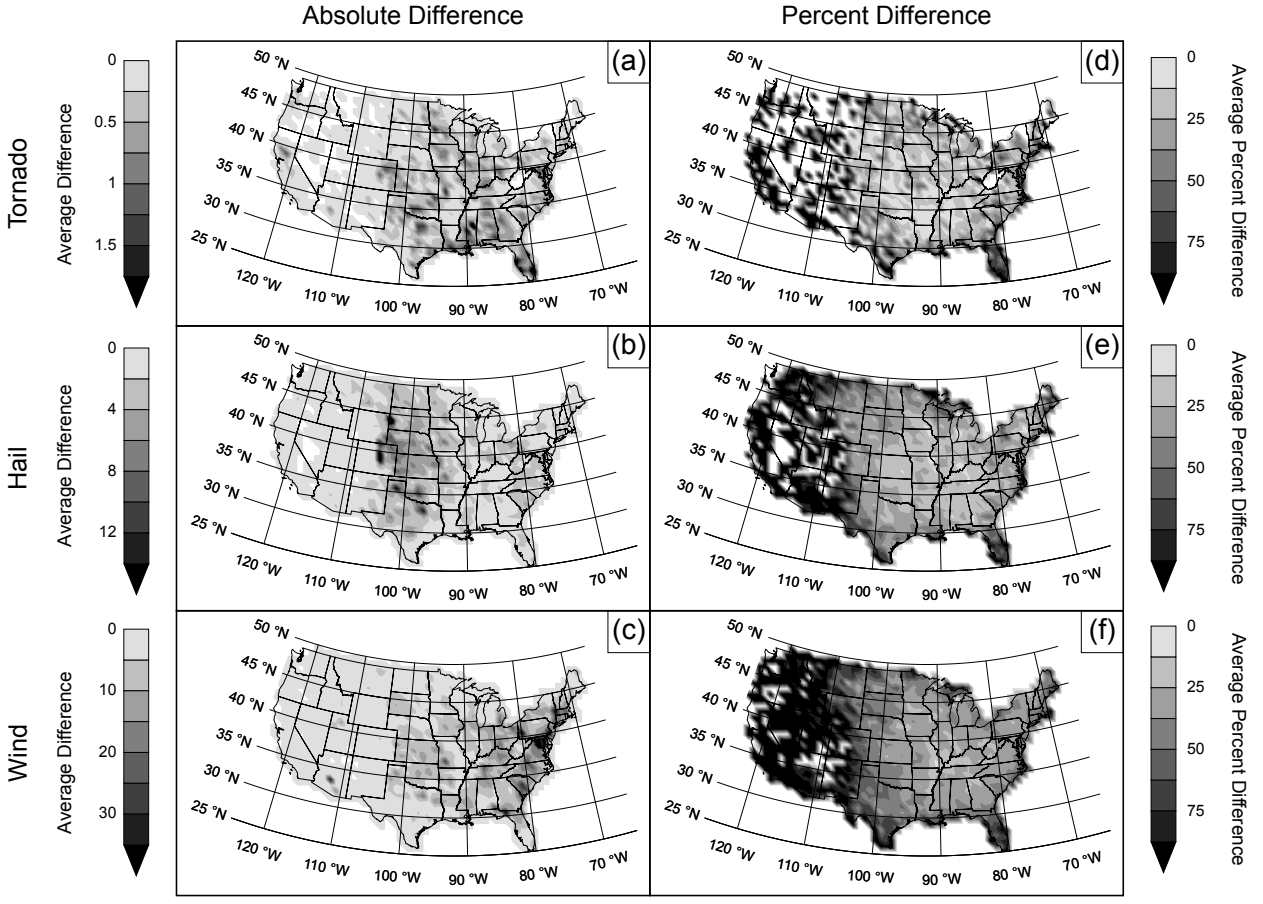

FIG. 7. Contour plots of average annual (a-c) absolute difference and (d-f) percent difference between GR-S and SED reports, for (a,d) tornado, (b,e) severe hail, and (c,f) severe wind reports from 2010-2019, inclusive. Data are gridded on an approximately 80×80 km grid. Areas not shaded indicate either no reports (both SED and GR-S) or an equal number of SED and GR-S reports.

Accepted for publication in *Monthly Weather Review*. DOI 10.1175/MWR-D-23-0017.1.

Confident that the GR-S database is representative of the seasonality and geographic distribution of SED reports, we can use GR-S data to examine other bulk aspects of storm severity. Identifying both the storm mode and updraft type (mesocyclonic or non-mesocyclonic) associated with each tracked storm and its matched reports can provide valuable insight into the types of storms that produce various severe phenomena. Figure 8 shows the average annual number of tornado, hail, and wind reports per month for 2010-2019, broken into sub-significant and significant severe reports. Overlaid are lines showing the percent of reports per month that were matched with storms classified as single cell, multicell, or MCS storms, and whether or not the storm had a mesocyclonic updraft. Perhaps the most surprising result from this analysis is how often tornadoes are associated with MCS-classified cells throughout the year (Fig. 8a). However, the mesocyclonic classfication reveals that many of the cells classified as MCS-type are dynamically consistent with supercell storms rather than the typical non-mesocyclonic cells often found in an MCS. We speculate that this may be driven by the reliance on a relatively low Z_{H} threshold to define storm contours during storm mode classification (Z_{H} = 30 dBZ), which may encompass the precipitation shield of neighboring–and otherwise mostly discrete–storms (supercell or otherwise) and classify those storms as part of an MCS. The contribution of non-mesocyclonic (i.e., more traditional) MCS cells to tornado reports reaches a minimum in the spring and summer, when both the number of tornadoes peaks and the classical U.S. tornado season occurs. In contrast, the contribution of mesocyclonic storms to tornado reports, regardless of storm mode classification, peaks during this time.

Examining hail events (Fig. 8b), for much of the spring through fall, single cell storms account for the largest fraction of reports by storm mode. However, while tornado and wind reports are fairly dominated by one storm mode (MCSs are associated with a majority of reports in 11 of 12 months for each tornadoes and wind), no one storm mode stands out as a consistent majority contributor to all hail reports. Single cell storms account for slightly more than 50% of reports in July and August; multicellular storms are never associated with the majority (or even a relative majority) of reports per month; and MCS storms make up a majority (50-64%) of reports only in the winter months, where total matched reports are lowest. However, examining mesocyclonic vs. non-mesocyclonic storms, mesocyclonic storms account for a majority of hail reports year-round. MCS storms contribute the most to wind reports year-round when compared to other storm modes

Accepted for publication in *Monthly Weather Review*. DOI 10.1175/MWR-D-23-0017.1.

(Fig. 8c), with a peak in single cell and multicell contribution in the late summer. This is when "severe weakly forced thunderstorms" (Miller and Mote 2017) are most common in the CONUS, which can cause downdraft-driven severe wind gusts (e.g., microbursts).

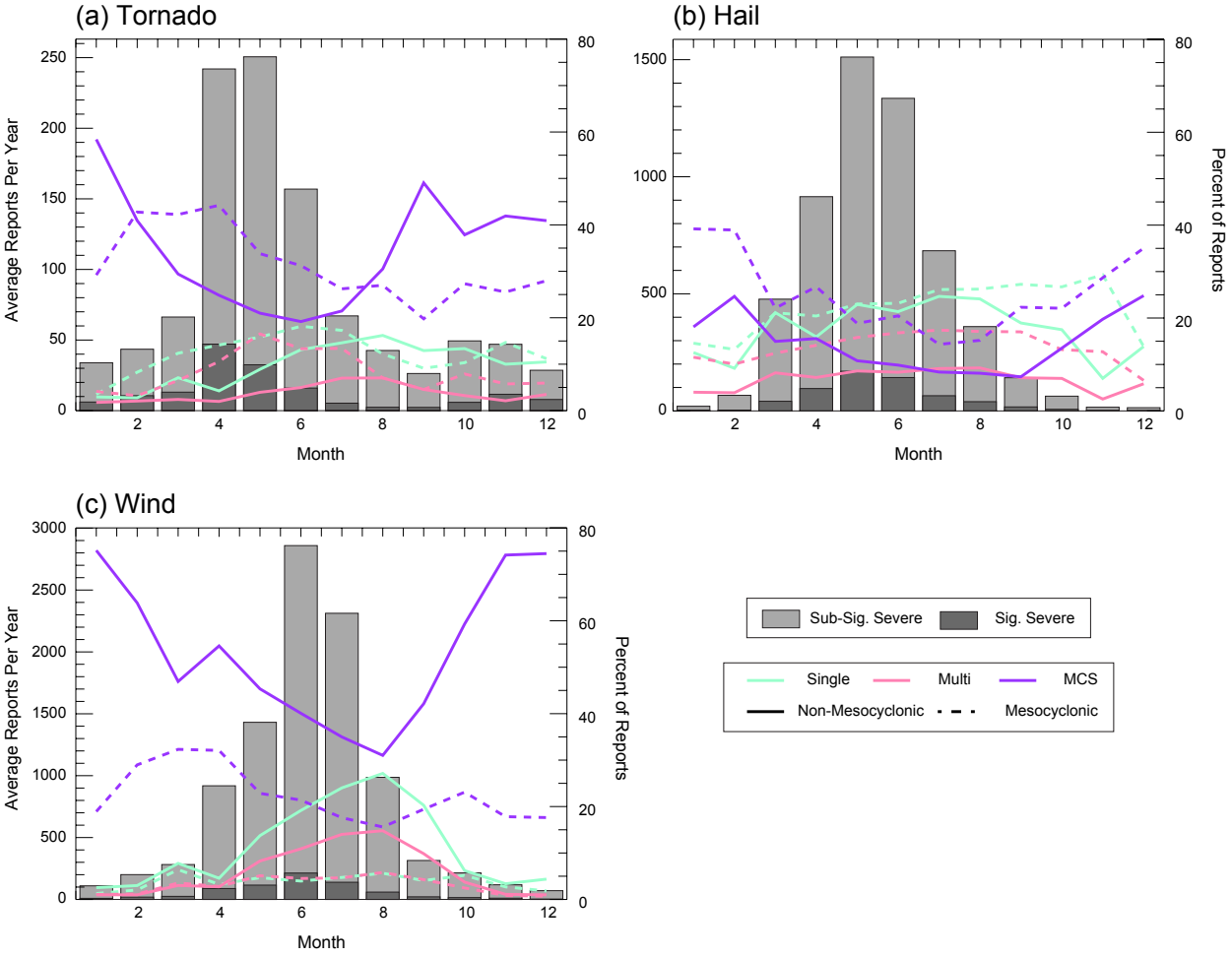

FIG. 8. Average annual number of GR-S matched (a) tornado, (b) severe hail, and (c) severe wind reports by month for 2010-2019. Lines show the percent of total reports that were matched to a storm of a given storm mode (single cell, multicell, or MCS; in green, pink, and purple, respectively) and with a given updraft type (non-mesocyclonic or mesocyclonic; in solid and dashed lines, respectively). Bar charts are split into lighter and darker gray, which show sub-significant severe and significant severe reports, respectively. The vertical extent of these two bars combined is the total number of all reports, and the sum of all lines in a given month is 100%.

Accepted for publication in *Monthly Weather Review*. DOI 10.1175/MWR-D-23-0017.1.

Similar to the annual cycle analysis, Fig. 9 reveals the average diurnal cycle of each hazard, relative to the reports' local solar noon. Solar noon is the time the sun aligns with a location's meridian, and using time relative to solar noon (as opposed to UTC time) eliminates the effect of time zones, providing a uniform representation of local time. Each severe report type has a pronounced diurnal cycle, with a peak in report frequency between approximately 2 and 8 hours after solar noon. During local nighttime, severe weather is associated most with MCS storm cells. As tornado reports increase in frequency after solar noon, the overall fraction of reports associated with MCSs drops (Fig. 9a). From 2 to 12 hours after solar noon, the majority of tornado reports for each of the three storm modes are produced from mesocyclonic storms. The hail data (Fig. 9b) show a more pronounced diurnal cycle when compared to tornadic and wind reports, with hail reports highly concentrated around their daily peak at 4-5 hours after solar noon. Single cell storms are the main contributor to hail reports in the first 7 hours after solar noon, with the contributions of multicellular and MCS storms nearly equal during those hours (~25%). Overall, mesocyclonic storms account for the majority of hail reports during 23 of the 24 total hours. As was true for the annual cycle, diurnal data show wind reports overwhelmingly associated with MCS storms throughout the majority of the day (Fig. 9c). MCSs are known to be prolific producers of damaging straight-line winds, so it is no surprise that these storms produce the most wind reports (a minimum of 48% of all wind reports each hour). Non-mesocyclonic single cell and multicell severe wind-producing storms have a pronounced peak in the hours after solar noon, which, as previously mentioned, is likely attributable to downdraft-driven wind gusts from severe weakly forced thunderstorms that are common in the late summer and early afternoon. Notably, mesocyclonic storms never account for a majority of severe wind reports throughout the day (< 39% of reports per hour), in contrast to how often they contribute to severe hail and tornado reports during the peak tornado- and hail-producing hours. For all analyses of the diurnal cycle of reports, note that the total number of reports may be lower during the overnight hours given that most people are asleep (e.g., Wendt and Jirak 2021).

Accepted for publication in *Monthly Weather Review*. DOI 10.1175/MWR-D-23-0017.1.

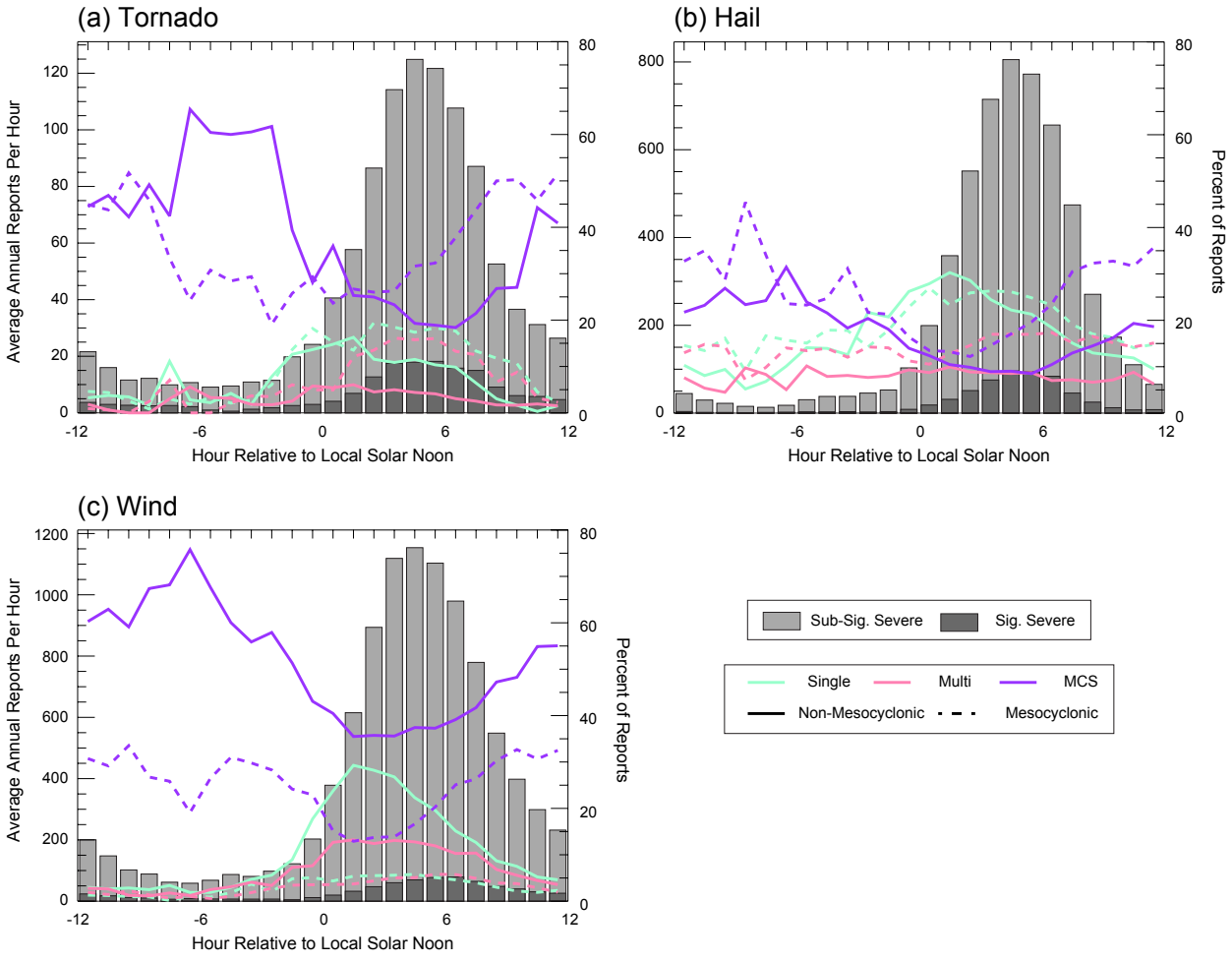

FIG. 9. Average annual number of GR-S matched (a) tornado, (b) severe hail, and (c) severe wind reports by hour relative to local solar noon for 2010-2019. Lines show the percent of total reports matched to a storm of a given storm mode (single cell, multicell, or MCS; in green, pink, and purple, respectively) and with a given updraft type (non-mesocyclonic or mesocyclonic; in solid and dashed lines, respectively). Bar charts are split into lighter and darker gray, which show sub-significant severe and significant severe reports, respectively. The vertical extent of these two bars combined is the total number of all reports, and the sum of all lines in a given hour is 100%.

Accepted for publication in *Monthly Weather Review*. DOI 10.1175/MWR-D-23-0017.1.

Finally, we can examine how storms of various modes and mesocyclonic/non-mesocyclonic classifications contribute to reports of varying magnitude. Figure 10 shows histograms of the magnitude of each report type and the fractional contribution of storms of a given storm mode and mesocyclonic/non-mesocyclonic classification. The data show that the vast majority of reports (> 90%) are sub-significant severe (i.e., below EF-2, 2", or 65 kts for tornado, hail, and wind reports, respectively). As EF rating increases, the relative contribution of mesocyclonic storms also increases, to the point where they are responsible for 90.5% and 100% of all EF-4 (84 total) and EF-5 (12 total) tornado reports in the database, respectively. In fact, for any EF rating, mesocyclonic storms account for the majority of tornadoes. GR-S data also show that EF-0, EF-1, and EF-2 tornadoes all predominantly come from cells embedded within MCSs (53.7, 73.4, and 65.6% of tornadoes, respectively). Focusing on significant tornadoes, the percent of tornadoes linked to MCS-classified storms decreases from 65.6% to 33.3% as the percent linked to single cell storms increases to a maximum of 58.3% for EF-5 tornadoes. Mesocyclonic storms are also the main contributor to hail reports, and hailstones are more likely to be associated with mesocyclonic storms as hail size increases. As was evident in Figs. 8 and 9, no one storm mode clearly dominates hail production. Interestingly, single cell storms account for a majority of hailstones in the lowest 3 bins, but contributions to 4"+ hailstones are relatively equal across storm modes. This comes with the caveat that the largest hailstone bin contains 0.7% of the total reports in the smallest hailstone bin. Wind reports become increasingly associated with mesocyclonic storms as wind speed increases, with the exception of the strongest winds in the dataset. These winds (95+ kts) are predominately from non-mesocyclonic storms (52.7%), in stark contrast with the strongest tornadoes and largest hail, which are overwhelmingly associated with mesocyclonic storms. Wind reports are largely dominated by storms embedded within MCSs, with 62.9-81.3% of reports in each bin attributed to MCSs. As touched on in the discussion of hail-producing storms, it is important to recognize that as EF rating, hail size, and wind speed increase, the sample size of reports decreases. Therefore, interpretation of mode and mesocyclonic/non-mesocyclonic breakdown must be done carefully, especially where sample sizes drop below a few hundred reports.

Accepted for publication in *Monthly Weather Review*. DOI 10.1175/MWR-D-23-0017.1.

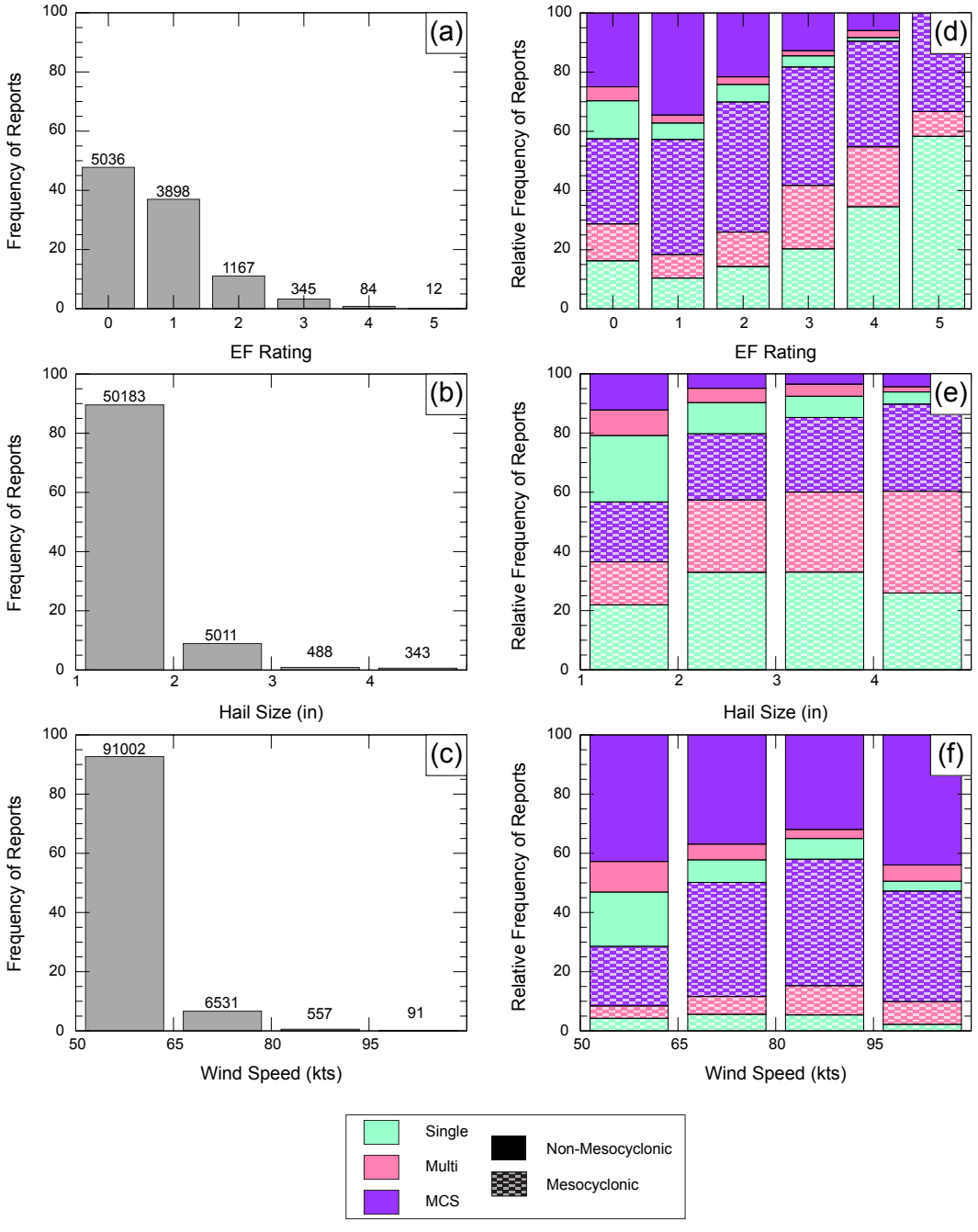

FIG. 10. Breakdown of (left; a-c) total frequency of reports by (a) EF rating, (b) hail size, and (c) wind speed, as well as (right; d-f) the percent of reports associated with a given combination of storm mode and supercell classification by (d) EF rating, (e) hail size, and (f) wind speed. On (a-c), the total number of reports in each bin are listed on top of the individual bars.

Accepted for publication in *Monthly Weather Review*. DOI 10.1175/MWR-D-23-0017.1.

5. Comparison to past studies

Given that GR-S storm-matched reports were demonstrated to be a representative sample of SED reports from 2010-2019, we can also use GR-S data to revisit analyses and conclusions from prior papers to assess reproducibility. Herein, we focus on two studies, Trapp et al. (2005) and Ashley et al. (2019), which examined the prevalence of various storm modes and their propensity to produce severe weather. Table 3 lists basic information about data sources and methods employed in the papers, as well as a summary of those used in the present study.

Storm Mode Classification Techniques			
Field	Trapp et al. (2005)	Ashley et al. (2019)	This Study
Years of Data:	1998–2000	1996–2017	2010–2019
Classification Technique:	Hand Analysis	Machine Learning	Objective Analysis
Z_H Data	Composite column-maximum images from NCDC (NCEI), other sources	NOWrad composite reflectivity data (Grassotti et al. 2003)	GR-S column-maximum data
Cell Classification:	Relatively isolated, circular or elliptical in shape, with $Z_{Hmax} \geq$ ~50 dBZ	—-	1 track in 30-dBZ Z_{Hmax} contour, or 2 tracks within 30-dBZ Z_{Hmax} contour < 3000 km^2
MCS Classification:	—-	Region of $Z_{Hmax} \geq 40$ dBZ persisting for at least 3 hours, with contiguous to semi-contiguous 40-dBZ contour maximum dimension ≥ 100 km	2 tracks within 30-dBZ Z_{Hmax} contour ≥ 3000 km^2 or 3+ tracks within 30-dBZ Z_{Hmax} contour. Maximum dimension ≥ 100 km
QLCS Classification:	Quasi-linear, $Z_{Hmax} \geq 40$ dBZ region with maximum dimension > 100 km	MCS with convective region aspect ratio ≥ 3	—-

TABLE 3. Comparison of techniques used to classify storm mode in past literature.

For comparisons between GR-S data and prior results focusing on MCS or QLCS storms, we will compare the papers' findings to only our non-mesocyclonic MCS cells. Comparing strictly our non-mesocyclonic MCS data to other studies' full MCS datasets resulted in greater consistency, potentially pointing to mesocyclonic MCS cells being more dynamically consistent with single cell mesocyclonic storms than with non-mesocyclonic MCS storms. This result is relevant to any future work using GR-S MCS data with the storm mode classification employed here. Also important to note is the delineation between an MCS and a QLCS. As discussed in Schumacher and Rasmussen (2020), a QLCS is a subset of the MCS archetype. While MCSs are typically defined as convective complexes with a maximum dimension ≥100 km, a QLCS is an MCS further characterized by an aspect ratio around 3:1, meaning that the system has one long and one short dimension. Given that the terms MCS and QLCS are often conflated, it is important to keep in mind the true nature

Accepted for publication in *Monthly Weather Review*. DOI 10.1175/MWR-D-23-0017.1.

of MCS-classified cells herein and how they may or may not be a part of a QLCS-type convective complex.

GR-S data are first compared to select conclusions from Trapp et al. (2005). The study's main goal was to "estimate the percentage of U.S. tornadoes that are spawned annually by squall lines and bow echoes, or quasi-linear convective systems (QLCSs)" using subjectively classified radar echoes over a three-year period (1998-2000, inclusive). Classification was done for QLCS and individual cells near the time of tornadogenesis per Table 3. They delineated between QLCS and cell type echoes based on "dynamics unique to these phenomena" and mentioned that, while tornadoes can form by mesocyclonic and non-mesocyclonic means, any distinction between cells producing tornadoes via these two different mechanisms was not investigated therein. Their final dataset included 3828 tornadoes.

Figure 11 shows reproductions of Trapp et al. (2005) Figs. 3b (Fig. 11a), 6 (Fig. 11b), and 8a (Fig. 11c) using GR-S data. Figure 11a shows the breakdown of the number of tornado reports by EF rating on a logarithmic scale for both single cell and MCS storms. Crucially, both MCS mesocyclonic and non-mesocyclonic lines are shifted such that they have an equal number of EF-2 reports per storm type; Fig. 11a therefore emphasizes the relative distributions of tornado intensity by storm type rather than absolute values. Trapp et al. (2005) found that there "appear to be disproportionately more F1 tornadoes from QLCSs, and more F3–F4 tornadoes from cells." Figure 11a shows this as well, where the non-mesocyclonic MCS cell line is above the single cell line for EF-1 tornadoes and below the cell line for EF 3-4 tornadoes. Here the mesocyclonic MCS curve more closely matches the single cell curve, pointing again to their dynamical similarities. On the other end of the spectrum, data from Trapp et al. (2005) (GR-S) show no F5 QLCS (EF-5 non-mesocyclonic MCS) tornadoes given they are quite rare, and also note that F5 (EF-5) tornadoes only comprise 0.2% (0.11%) of the total dataset. Trapp et al. (2005) also noted that their QLCS curve was fairly log-linear except for F0 tornadoes, potentially attributable to underreporting of the weakest tornadoes. This same linear shape, along with relatively low EF-0 tornado counts, is visible in the GR-S non-mesocyclonic MCS curve.

Figure 11b shows the cumulative distribution of all tornado reports broken down by month and storm type. Trapp et al. (2005) found that 32% of all QLCS tornado reports occurred within the first three months of the year, compared to just 14% of single cell reports. The lower relative

Accepted for publication in *Monthly Weather Review*. DOI 10.1175/MWR-D-23-0017.1.

fraction of cell reports compared to QLCS reports is mirrored with the GR-S data, with tornadoes in January-March making up 20% of non-mesocyclonic MCS tornadoes and just 8% of single cell tornadoes. Therefore, with both datasets, a higher proportion of annual MCS tornadoes occurred in the first three months of the year compared to the proportion of annual single cell tornadoes. Finally, Fig. 11c shows the diurnal cycle of tornado reports, using time relative to local solar noon. Trapp et al. (2005) found that cell reports peaked close to 18 local standard time (LST), with a similar albeit smaller peak in QLCS data near 18 LST. GR-S data show similar trends, with peaks in single cell and non-mesocyclonic MCS data between 3-5 hours after solar noon, and a higher peak for single cell than non-mesocyclonic MCS data (i.e., a more amplified diurnal cycle). Mesocyclonic MCS cells are again more consistent with single cell storms, with a ~2 hour offset in their diurnal cycle compared to the single cell data.

Accepted for publication in *Monthly Weather Review*. DOI 10.1175/MWR-D-23-0017.1.

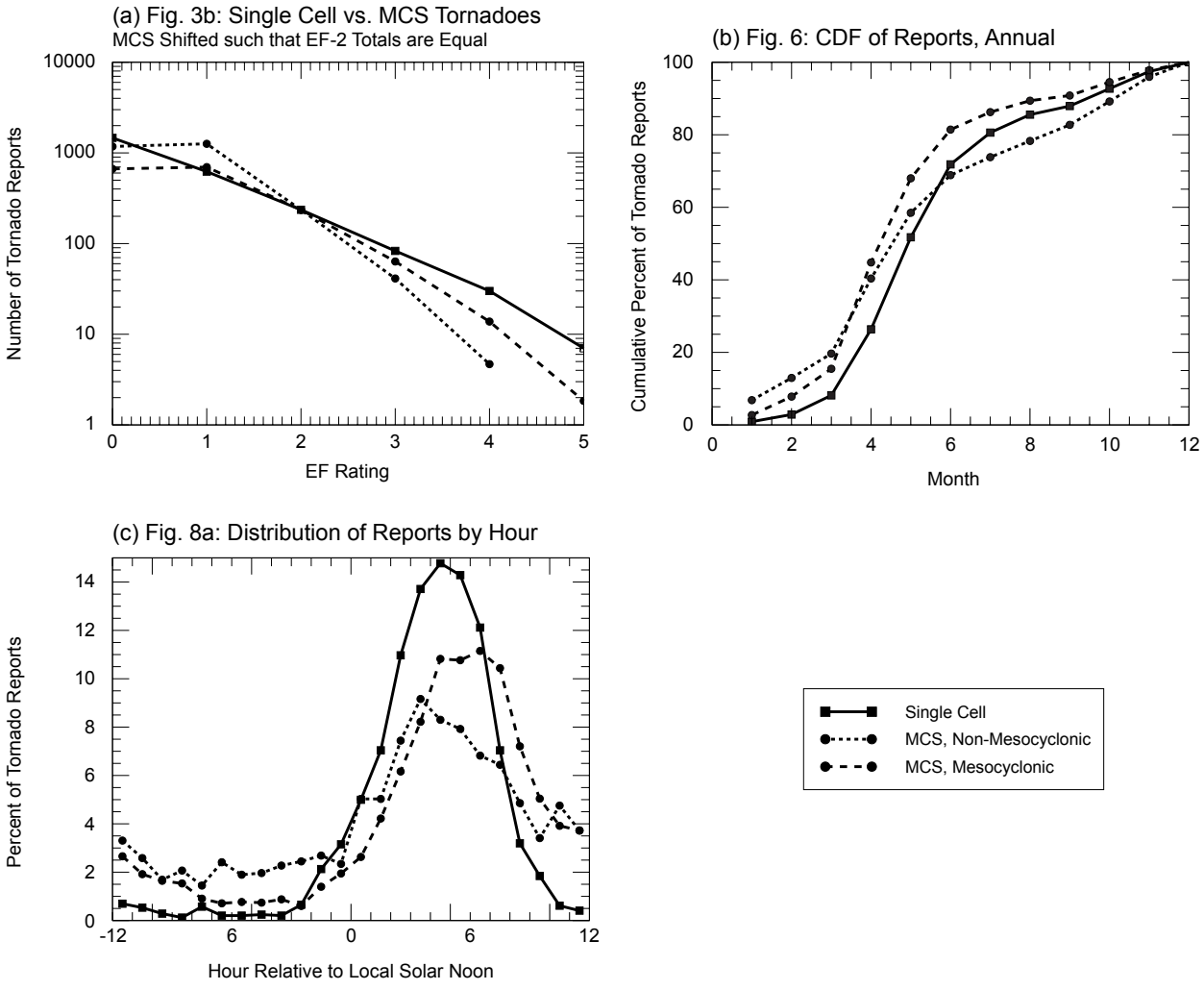

FIG. 11. Plots reproducing (a) Fig. 3b, (b) Fig. 6, and (c) Fig. 8a in Trapp et al. (2005) using GR-S data. Lines are broken into single cell storms, non-mesocyclonic MCS storms, and mesocyclonic MCS storms. On panel (c), data within each one-hour bin are plotted at the 30 minute mark of that hour.

Accepted for publication in *Monthly Weather Review*. DOI 10.1175/MWR-D-23-0017.1.

GR-S data are additionally compared to the findings of Ashley et al. (2019), who used machine learning methods to classify storm mode using a 22-year radar dataset. For training the model, QLCS storms were labeled by hand, and the model was trained on labeled QLCS and non-QLCS events. They defined an MCS per Table 3, with that definition motivated primarily by the work of Parker and Johnson (2000). A QLCS is defined as "an MCS that has instantaneous convective (≥40 dBZ) regions that are longer than 100 km and must be at least 3 times as long as they are wide." The major differences between their definition of an MCS and the definition used herein is the 30- vs. 40-dBZ threshold for defining radar echoes for classification, and no temporal threshold vs. a 3 hour temporal threshold for GR-S and Ashley et al. (2019), respectively. Their paper focuses on the spatiotemporal distribution of both QLCSs and QLCS-matched tornado reports, and only the latter will be analyzed herein.

Table 4 shows the percent contribution of severe reports attributable to QLCSs in Ashley et al. (2019) juxtaposed with storm-matched GR-S reports attributable to non-mesocyclonic MCS cells. In each category, the percent of reports attributed to MCSs is fairly similar when comparing GR-S data to the results in Ashley et al. (2019). The greatest difference is with attribution of significant severe wind reports (28% of storms in Ashley et al. (2019) vs. ~42% in GR-S). Although trends in these data are similar, differences are no doubt the result of a myriad of differences in methods throughout the data analysis process. Both datasets show a high percentage of wind reports and a low percentage of hail reports attributed to QLCS/non-mesocyclonic MCS storms. Beyond examining total reports attributed to QLCSs, their Fig. 11 shows a breakdown of all severe reports by month and hour, with percent attributed to QLCSs overlaid. Similar to Fig. 8 herein, they found tornado and hail reports peak in the late spring and wind reports peak in the early summer. They also found that QLCS contribution to total reports was maximized during the winter months and minimized in late summer/early fall, which was similar to the summer/early fall minima and wintertime maxima seen in the non-mesocyclonic MCS GR-S data. Examining their hourly data, they found a minimum in QLCS contribution during times of peak reporting (~18-03 UTC), which, when examining GR-S data binned by local time (in UTC, not shown), non-mesocyclonic MCS contributions are minimized from 20-04 UTC for tornadoes and from 17-03 UTC for hail and wind reports. The average percent contribution of QLCSs to hail reports in their study was lower than that for wind and tornado reports, which is also reflected in the GR-S data. Overall, the similarities

Accepted for publication in *Monthly Weather Review*. DOI 10.1175/MWR-D-23-0017.1.

Comparison of Percent of Severe and Sig. Severe Reports Attributed to MCSs/QLCSs		
Report Type and Severity	GridRad-Severe MCS	Ashley et al. (2019) QLCS
Tornado, Severe:	27.54%	21%
Tornado, Sig. Severe:	18.72%	26%
Hail, Severe:	11.43%	10%
Hail, Sig. Severe:	4.74%	7%
Wind, Severe:	42.31%	28%
Wind, Sig. Severe:	36.61%	34%

TABLE 4. Comparison of percent of reports attributable to MCSs for different report types and severity. Data shown are from Ashley et al. (2019) and GR-S data.

between GR-S conclusions and those of Trapp et al. (2005) and Ashley et al. (2019) point to the efficacy of the GR-S techniques as a whole and the storm mode classification algorithms used herein.

6. Conclusions

In this study, the GR-S dataset was introduced, a dataset centered on CONUS-wide radar data for ~100 of the most severe days per year from 2010-2019, inclusive. After determining which days to include in the database, spatiotemporal domains for radar data are selected objectively, and all storms within the domain are tracked throughout their lifetimes. Storms are matched with severe reports and both storm mode classification (single cell, multicell, or MCS) and supercell classification (mesocyclonic or non-mesocyclonic, for all three storm modes) are performed. Based on the analysis presented, the following conclusions can be drawn:

1) The GR-S dataset captures a majority of SED reports from 2010-2019 inclusive, and captures ~90% of reports that exist within the spatiotemporal bounds of GR-S (Table 2). The reports captured are analogous in spatial and temporal distribution to the SED reports, and the relative contribution of tornado, hail, and wind reports to all reports per month also mirror that of the SED database quite well (Figs. 5–7). Therefore, the storm-matched reports within the GR-S database are a representative sample of the complete SED dataset.

2) Pronounced annual and diurnal variability was evident for tornado, hail, and wind reports: (i) MCS-classified cells produced the most tornadoes throughout the entire year when compared to other storm modes, and mesocyclonic storms were found to be the primary tornado contributors during peak tornado frequency in spring and summer (Fig. 8a). During the overnight and early

Accepted for publication in *Monthly Weather Review*. DOI 10.1175/MWR-D-23-0017.1.

morning when total number of reports is low, MCS contribution is maximized, and during the time of peak reports, mesocyclonic storms produce the majority of tornado reports (Fig. 9a). (ii) Single cell storms account for the largest fraction of hail reports by storm mode for spring through fall, and mesocyclonic storms account for a majority of all hail reports both year-round (Fig. 8b) and throughout the day (Fig. 9b). Hail reports have the most pronounced diurnal cycle of the three report types, meaning that reports are highly concentrated around their time of peak occurrence (~4-5 hours after local solar noon). Unlike tornadoes and wind reports, there is no one storm mode that stands out as the primary producer of severe hail reports over the whole year or whole day. (iii) MCS-classified cells produce the most severe wind reports throughout the entire year (Fig. 8c) and day (Fig. 9c) when compared to other storm modes. There is a peak in non-mesocyclonic single cell and multicell contribution to wind reports in the late summer and early afternoon, likely due to decay of severe weakly forced thunderstorms.

3) For both tornado and hail reports, as EF-rating and hail size increase, so does the relative contribution of mesocyclonic storms to total reports (Fig. 10). Wind reports show a similar trend, but the contribution of mesocyclonic storms does not monotonically increase with increasing wind speed. However, due to small sample sizes at the highest intensities, such breakdowns should be interpreted carefully.

4) GR-S was found to broadly reproduce the findings of Trapp et al. (2005) (Fig. 11) and Ashley et al. (2019) (Table 4), lending credence to the usefulness of the GR-S dataset and quality of storm mode classification applied herein.

The GR-S database was created to facilitate robust studies of severe weather using radar data from a large sample of storms. Namely, the objective methods used to build the now-public dataset (School of Meteorology, University of Oklahoma 2021) provide an opportunity to easily investigate thousands of severe storms and over 1.3 million total storms with great detail. We believe these data can be used to examine several challenging and important science questions regarding severe weather and we encourage others to use GR-S to explore their own scientific questions as the dataset continues to grow.

Accepted for publication in *Monthly Weather Review*. DOI 10.1175/MWR-D-23-0017.1.

Acknowledgments. We thank Emily Tinney and Dr. Elisa Murillo for advice on figures shown herein, which were designed to be equally interpretable to individuals with full color vision and individuals with color vision deficiency. We also thank Dr. Matthew Bunkers, Dr. Zhe Feng, and one anonymous reviewer for their thoughtful comments, which helped improve the clarity and quality of the manuscript. This material is based upon work supported by the National Science Foundation under Grant No. ICER-2019758 and the NOAA Weather Program Office Joint Technology Transfer Initiative grant NA20OAR4590356 to the University of Oklahoma. This work is part of the NSF AI Institute for Research on Trustworthy AI in Weather, Climate, and Coastal Oceanography (AI2ES).

Data availability statement. Radar data are publicly accessible through the National Centers for Environmental Information (NOAA/NWS/ROC 1991), and storm reports can be accessed from the Storm Events Database (NCEI/NOAA 2022). Processed GR-S data are publicly available via the Research Data Archive at the National Center for Atmospheric Research, Computational and Information Systems Laboratory (School of Meteorology, University of Oklahoma 2021).

References

Allen, J. T., and M. K. Tippett, 2015: The characteristics of united states hail reports: 1955-2014. *Electronic J./ Severe Storms Meteor.*, **10 (3)**, 1 – 31.

Anderson-Frey, A. K., and H. Brooks, 2019: Tornado fatalities: An environmental perspective. *Weather and Forecasting*, **34**, 1999 – 2015, https://doi.org/10.1175/WAF-D-19-0119.1, URL https://journals.ametsoc.org/view/journals/wefo/34/6/waf-d-19-0119_1.xml.

Ashley, W. S., A. M. Haberlie, and J. Strohm, 2019: A climatology of quasi-linear convective systems and their hazards in the united states. *Weather and Forecasting*, **34**, 1605 – 1631, https://doi.org/10.1175/WAF-D-19-0014.1, URL https://journals.ametsoc.org/view/journals/wefo/34/6/waf-d-19-0014_1.xml.

Ashley, W. S., A. J. Krmenec, and R. Schwantes, 2008: Vulnerability due to nocturnal tornadoes. *Weather and Forecasting*, **23**, 795 – 807, https://doi.org/10.1175/2008WAF2222132.1, URL https://journals.ametsoc.org/view/journals/wefo/23/5/2008waf2222132_1.xml.

Accepted for publication in *Monthly Weather Review*. DOI 10.1175/MWR-D-23-0017.1.

Bentley, M. L., and T. L. Mote, 1998: A climatology of derecho-producing mesoscale convective systems in the central and eastern united states, 1986–95. part i: Temporal and spatial distribution. *Bulletin of the American Meteorological Society*, **79**, 2527 – 2540, https://doi.org/10.1175/1520-0477(1998)079⟨2527:ACODPM⟩2.0.CO;2, URL https://journals.ametsoc.org/view/journals/bams/79/11/1520-0477_1998_079_2527_acodpm_2_0_co_2.xml.

Blair, S. F., D. R. Deroche, J. M. Boustead, J. W. Leighton, B. L. Barjenbruch, and W. P. Gargan, 2011: A radar-based assessment of the detectability of giant hail. *Electronic J. Severe Storms Meteor.*, **6 (7)**, 1–30.

Bluestein, H. B., and M. H. Jain, 1985: Formation of mesoscale lines of pirecipitation: Severe squall lines in oklahoma during the spring. *Journal of Atmospheric Sciences*, **42**, 1711 – 1732, https://doi.org/10.1175/1520-0469(1985)042⟨1711:FOMLOP⟩2.0.CO;2, URL https://journals.ametsoc.org/view/journals/atsc/42/16/1520-0469_1985_042_1711_fomlop_2_0_co_2.xml.

Bluestein, H. B., and S. S. Parker, 1993: Modes of isolated, severe convective storm formation along the dryline. *Monthly Weather Review*, **121**, 1354 – 1372, https://doi.org/10.1175/1520-0493(1993)121⟨1354:MOISCS⟩2.0.CO;2, URL https://journals.ametsoc.org/view/journals/mwre/121/5/1520-0493_1993_121_1354_moiscs_2_0_co_2.xml.

Brooks, H., and C. A. Doswell, 2001: Some aspects of the international climatology of tornadoes by damage classification. *Atmospheric Research*, **56 (1)**, 191–201, https://doi.org/https://doi.org/10.1016/S0169-8095(00)00098-3, URL https://www.sciencedirect.com/science/article/pii/S0169809500000983, conference on European Tornadoes and Severe Storms.

Brooks, H. E., C. A. Doswell, and M. P. Kay, 2003: Climatological estimates of local daily tornado probability for the united states. *Weather and Forecasting*, **18**, 626 – 640, https://doi.org/10.1175/1520-0434(2003)018⟨0626:CEOLDT⟩2.0.CO;2, URL https://journals.ametsoc.org/view/journals/wefo/18/4/1520-0434_2003_018_0626_ceoldt_2_0_co_2.xml.

Brown, R. A., L. R. Lemon, and D. W. Burgess, 1978: Tornado detection by pulsed doppler radar. *Monthly Weather Review*, **106**, 29 – 38, https://doi.org/10.1175/1520-0493(1978)106⟨0029:TDBPDR⟩2.0.CO;2, URL https://journals.ametsoc.org/view/journals/mwre/106/1/1520-0493_1978_106_0029_tdbpdr_2_0_co_2.xml.

Accepted for publication in *Monthly Weather Review*. DOI 10.1175/MWR-D-23-0017.1.

Browning, K. A., 1964: Airflow and precipitation trajectories within severe local storms which travel to the right of the winds. *Journal of Atmospheric Sciences*, **21**, 634 – 639, https://doi.org/10.1175/1520-0469(1964)021⟨0634:AAPTWS⟩2.0.CO;2, URL https://journals.ametsoc.org/view/journals/atsc/21/6/1520-0469_1964_021_0634_aaptws_2_0_co_2.xml.

Bunkers, M. J., M. R. Hjelmfelt, and P. L. Smith, 2006: An observational examination of long-lived supercells. part i: Characteristics, evolution, and demise. *Weather and Forecasting*, **21**, 673 – 688.

Byers, H. R., and R. R. Braham, 1949: The thunderstorm: Report of the thunderstorm project. URL https://books.google.com/books/about/The_Thunderstorm.html?id=D8sJAQAAIAAJ, U.S. Government Printing Office.

Cintineo, J. L., T. M. Smith, V. Lakshmanan, H. E. Brooks, and K. L. Ortega, 2012: An objective high-resolution hail climatology of the contiguous united states. *Weather and Forecasting*, **27**, 1235 – 1248, https://doi.org/10.1175/WAF-D-11-00151.1, URL https://journals.ametsoc.org/view/journals/wefo/27/5/waf-d-11-00151_1.xml.

Coleman, T. A., and P. G. Dixon, 2014: An objective analysis of tornado risk in the united states. *Weather and Forecasting*, **29**, 366 – 376, https://doi.org/10.1175/WAF-D-13-00057.1, URL https://journals.ametsoc.org/view/journals/wefo/29/2/waf-d-13-00057_1.xml.

Coniglio, M. C., S. F. Corfidi, and J. S. Kain, 2011: Environment and early evolution of the 8 may 2009 derecho-producing convective system. *Monthly Weather Review*, **139**, 1083 – 1102, https://doi.org/https://doi.org/10.1175/2010MWR3413.1, URL https://journals.ametsoc.org/view/journals/mwre/139/4/2010mwr3413.1.xml.

Coniglio, M. C., and D. J. Stensrud, 2004: Interpreting the climatology of derechos. *Weather and Forecasting*, **19**, 595 – 605, https://doi.org/10.1175/1520-0434(2004)019⟨0595:ITCOD⟩2.0.CO;2, URL https://journals.ametsoc.org/view/journals/wefo/19/3/1520-0434_2004_019_0595_itcod_2_0_co_2.xml.

Corfidi, S. F., M. C. Coniglio, A. E. Cohen, and C. M. Mead, 2016: A proposed revision to the definition of "derecho". *Bulletin of the American Meteorological Society*, **97**, 935

Accepted for publication in *Monthly Weather Review*. DOI 10.1175/MWR-D-23-0017.1.

– 949, https://doi.org/10.1175/BAMS-D-14-00254.1, URL https://journals.ametsoc.org/view/journals/bams/97/6/bams-d-14-00254.1.xml.

Crum, T. D., and R. L. Alberty, 1993: The wsr-88d and the wsr-88d operational support facility. *Bulletin of the American Meteorological Society*, **74**, 1669 – 1688, https://doi.org/10.1175/1520-0477(1993)074⟨1669:TWATWO⟩2.0.CO;2, URL https://journals.ametsoc.org/view/journals/bams/74/9/1520-0477_1993_074_1669_twatwo_2_0_co_2.xml.

DeWald, V. L., and T. W. Funk, 2002: Wsr-88d reflectivity and velocity trends of a damaging squall line event on 20 april 1996 over south-central indiana and central kentucky. *20th Conf. on Severe Local Storms*, American Meteorological Society, 177–180, 6.3.

Doswell, C. A., H. E. Brooks, and N. Dotzek, 2009: On the implementation of the enhanced fujita scale in the usa. *Atmospheric Research*, **93 (1)**, 554–563, https://doi.org/https://doi.org/10.1016/j.atmosres.2008.11.003, URL https://www.sciencedirect.com/science/article/pii/S0169809508003438, 4th European Conference on Severe Storms.

Edwards, R., J. G. LaDue, J. T. Ferree, K. Scharfenberg, C. Maier, and W. L. Coulbourne, 2013: Tornado intensity estimation: Past, present, and future. *Bulletin of the American Meteorological Society*, **94**, 641 – 653, https://doi.org/10.1175/BAMS-D-11-00006.1, URL https://journals.ametsoc.org/view/journals/bams/94/5/bams-d-11-00006.1.xml.

Feng, Z., R. A. Houze, L. R. Leung, F. Song, J. C. Hardin, J. Wang, W. I. Gustafson, and C. R. Homeyer, 2019: Spatiotemporal characteristics and large-scale environments of mesoscale convective systems east of the rocky mountains. *Journal of Climate*, **32**, 7303 – 7328, https://doi.org/https://doi.org/10.1175/JCLI-D-19-0137.1, URL https://journals.ametsoc.org/view/journals/clim/32/21/jcli-d-19-0137.1.xml.

Feng, Z., L. R. Leung, R. A. Houze Jr., S. Hagos, J. Hardin, Q. Yang, B. Han, and J. Fan, 2018: Structure and evolution of mesoscale convective systems: Sensitivity to cloud microphysics in convection-permitting simulations over the united states. *Journal of Advances in Modeling Earth Systems*, **10 (7)**, 1470–1494, https://doi.org/https://doi.org/10.1029/2018MS001305, URL https://agupubs.onlinelibrary.wiley.com/doi/abs/10.1029/2018MS001305, https://agupubs.onlinelibrary.wiley.com/doi/pdf/10.1029/2018MS001305.

Accepted for publication in *Monthly Weather Review*. DOI 10.1175/MWR-D-23-0017.1.

Fowle, M. A., and P. J. Roebber, 2003: Short-range (0–48 h) numerical prediction of convective occurrence, mode, and location. *Weather and Forecasting*, **18**, 782 – 794, https://doi.org/10.1175/1520-0434(2003)018⟨0782:SHNPOC⟩2.0.CO;2, URL https://journals.ametsoc.org/view/journals/wefo/18/5/1520-0434_2003_018_0782_shnpoc_2_0_co_2.xml.

Fujita, T. T., 1990: Downbursts: meteorological features and wind field characteristics. *Journal of Wind Engineering and Industrial Aerodynamics*, **36**, 75–86, https://doi.org/https://doi.org/10.1016/0167-6105(90)90294-M, URL https://www.sciencedirect.com/science/article/pii/016761059090294M, the Sixth U.S. National Conference on Wind Engineering.

Fujita, T. T., and H. R. Byers, 1977: Spearhead echo and downburst in the crash of an airliner. *Monthly Weather Review*, **105**, 129 – 146, https://doi.org/10.1175/1520-0493(1977)105⟨0129:SEADIT⟩2.0.CO;2, URL https://journals.ametsoc.org/view/journals/mwre/105/2/1520-0493_1977_105_0129_seadit_2_0_co_2.xml.

Fujita, T. T., and R. M. Wakimoto, 1982: Effects of miso- and mesoscale obstructions on pam winds obtained during project nimrod. *Journal of Applied Meteorology and Climatology*, **21**, 840 – 858, https://doi.org/10.1175/1520-0450(1982)021⟨0840:EOMAMO⟩2.0.CO;2, URL https://journals.ametsoc.org/view/journals/apme/21/6/1520-0450_1982_021_0840_eomamo_2_0_co_2.xml.

Gallus, W. A., N. A. Snook, and E. V. Johnson, 2008: Spring and summer severe weather reports over the midwest as a function of convective mode: A preliminary study. *Weather and Forecasting*, **23**, 101 – 113, https://doi.org/10.1175/2007WAF2006120.1, URL https://journals.ametsoc.org/view/journals/wefo/23/1/2007waf2006120_1.xml.

Geerts, B., 1998: Mesoscale convective systems in the southeast united states during 1994–95: A survey. *Weather and Forecasting*, **13**, 860 – 869, https://doi.org/https://doi.org/10.1175/1520-0434(1998)013⟨0860:MCSITS⟩2.0.CO;2, URL https://journals.ametsoc.org/view/journals/wefo/13/3/1520-0434_1998_013_0860_mcsits_2_0_co_2.xml.

Gensini, V. A., and H. E. Brooks, 2018: Spatial trends in united states tornado frequency. *npj Climate and Atmospheric Science*, **1 (38)**, 1 – 5, URL https://doi.org/10.1038/s41612-018-0048-2.

Accepted for publication in *Monthly Weather Review*. DOI 10.1175/MWR-D-23-0017.1.

Grassotti, C., R. N. Hoffman, E. R. Vivoni, and D. Entekhabi, 2003: Multiple-timescale intercomparison of two radar products and rain gauge observations over the arkansas–red river basin. *Weather and Forecasting*, **18**, 1207 – 1229.

Gutierrez, R. E., and M. R. Kumjian, 2021: Environmental and radar characteristics of gargantuan hail–producing storms. *Monthly Weather Review*, **149**, 2523 – 2538, https://doi.org/10.1175/MWR-D-20-0298.1, URL https://journals.ametsoc.org/view/journals/mwre/149/8/MWR-D-20-0298.1.xml.

Hales Jr., J. E., 1988: Improving the watch/warning program through use of significant event data. Preprints, 15th Conf. on Severe Local Storms, Baltimore, MD, Amer. Meteor. Soc., 165–168.

Homeyer, C. R., and K. P. Bowman, 2022: Algorithm description document for version 4.2 of the three-dimensional gridded nexrad wsr-88d radar (gridrad) dataset. URL http://gridrad.org/pdf/GridRad-v4.2-Algorithm-Description.pdf.

Homeyer, C. R., J. D. McAuliffe, and K. M. Bedka, 2017: On the development of above-anvil cirrus plumes in extratropical convection. *Journal of the Atmospheric Sciences*, **74**, 1617 – 1633, https://doi.org/10.1175/JAS-D-16-0269.1, URL https://journals.ametsoc.org/view/journals/atsc/74/5/jas-d-16-0269.1.xml.

Homeyer, C. R., T. N. Sandmæl, C. K. Potvin, and A. M. Murphy, 2020: Distinguishing characteristics of tornadic and nontornadic supercell storms from composite mean analyses of radar observations. *Monthly Weather Review*, **148**, 5015 – 5040, https://doi.org/10.1175/MWR-D-20-0136.1, URL https://journals.ametsoc.org/view/journals/mwre/148/12/mwr-d-20-0136.1.xml.

Houze Jr., R. A., 2004: Mesoscale convective systems. *Reviews of Geophysics*, **42 (4)**, https://doi.org/https://doi.org/10.1029/2004RG000150, URL https://agupubs.onlinelibrary.wiley.com/doi/abs/10.1029/2004RG000150, https://agupubs.onlinelibrary.wiley.com/doi/pdf/10.1029/2004RG000150.

Hurlbut, M. M., and A. E. Cohen, 2014: Environments of northeast u.s. severe thunderstorm events from 1999 to 2009. *Weather and Forecasting*, **29**, 3 – 22, https://doi.org/10.1175/WAF-D-12-00042.1, URL https://journals.ametsoc.org/view/journals/wefo/29/1/waf-d-12-00042_1.xml.

Accepted for publication in *Monthly Weather Review*. DOI 10.1175/MWR-D-23-0017.1.

Johns, R. H., and W. D. Hirt, 1987: Derechos: Widespread convectively induced windstorms. *Weather and Forecasting*, **2**, 32 – 49, https://doi.org/10.1175/1520-0434(1987)002⟨0032:DWCIW⟩2.0.CO;2, URL https://journals.ametsoc.org/view/journals/wefo/2/1/1520-0434_1987_002_0032_dwciw_2_0_co_2.xml.

Klimowski, B. A., M. J. Bunkers, M. R. Hjelmfelt, and J. N. Covert, 2003: Severe convective windstorms over the northern high plains of the united states. *Weather and Forecasting*, **18**, 502 – 519, https://doi.org/10.1175/1520-0434(2003)18⟨502:SCWOTN⟩2.0.CO;2, URL https://journals.ametsoc.org/view/journals/wefo/18/3/1520-0434_2003_18_502_scwotn_2_0_co_2.xml.

Krocak, M. J., and H. E. Brooks, 2018: Climatological estimates of hourly tornado probability for the united states. *Weather and Forecasting*, **33**, 59 – 69, https://doi.org/10.1175/WAF-D-17-0123.1, URL https://journals.ametsoc.org/view/journals/wefo/33/1/waf-d-17-0123_1.xml.

Kumjian, M. R., 2013: Principles and applications of dual-polarization weather radar. part ii: Warm- and cold-season applications. *Journal of Operational Meteorology*, **1 (20)**, 243 – 264.

Kumjian, M. R., and A. V. Ryzhkov, 2008: Polarimetric signatures in supercell thunderstorms. *Journal of Applied Meteorology and Climatology*, **47**, 1940 – 1961, https://doi.org/10.1175/2007JAMC1874.1, URL https://journals.ametsoc.org/view/journals/apme/47/7/2007jamc1874.1.xml.

Kurdzo, J. M., and Coauthors, 2017: Observations of severe local storms and tornadoes with the atmospheric imaging radar. *Bulletin of the American Meteorological Society*, **98**, 915 – 935, https://doi.org/10.1175/BAMS-D-15-00266.1, URL https://journals.ametsoc.org/view/journals/bams/98/5/bams-d-15-00266.1.xml.

Lagerquist, R., A. McGovern, C. R. Homeyer, D. J. G. II, and T. Smith, 2020: Deep learning on three-dimensional multiscale data for next-hour tornado prediction. *Monthly Weather Review*, **148**, 2837 – 2861, https://doi.org/10.1175/MWR-D-19-0372.1, URL https://journals.ametsoc.org/view/journals/mwre/148/7/mwrD190372.xml.

Lemon, L. R., and C. A. Doswell, 1979: Severe thunderstorm evolution and mesocyclone structure as related to tornadogenesis. *Monthly Weather Review*, **107**, 1184 – 1197, https://doi.org/10.

Accepted for publication in *Monthly Weather Review*. DOI 10.1175/MWR-D-23-0017.1.

1175/1520-0493(1979)107⟨1184:STEAMS⟩2.0.CO;2, URL https://journals.ametsoc.org/view/journals/mwre/107/9/1520-0493_1979_107_1184_steams_2_0_co_2.xml.

Loeffler, S. D., M. R. Kumjian, M. Jurewicz, and M. M. French, 2020: Differentiating between tornadic and nontornadic supercells using polarimetric radar signatures of hydrometeor size sorting. *Geophysical Research Letters*, **47 (12)**, https://doi.org/10.1029/2020GL088242.

McCarthy, J., J. W. Wilson, and T. T. Fujita, 1982: The joint airport weather studies project. *Bulletin of the American Meteorological Society*, **63**, 15 – 22, https://doi.org/10.1175/1520-0477(1982)063⟨0015:TJAWSP⟩2.0.CO;2, URL https://journals.ametsoc.org/view/journals/bams/63/1/1520-0477_1982_063_0015_tjawsp_2_0_co_2.xml.

Miller, P. W., and T. L. Mote, 2017: Standardizing the definition of a "pulse" thunderstorm. *Bulletin of the American Meteorological Society*, **98**, 905 – 913, https://doi.org/10.1175/BAMS-D-16-0064.1, URL https://journals.ametsoc.org/view/journals/bams/98/5/bams-d-16-0064.1.xml.

Murillo, E. M., and C. R. Homeyer, 2019: Severe hail fall and hailstorm detection using remote sensing observations. *Journal of Applied Meteorology and Climatology*, **58**, 947 – 970, https://doi.org/10.1175/JAMC-D-18-0247.1, URL https://journals.ametsoc.org/view/journals/apme/58/5/jamc-d-18-0247.1.xml.

Murillo, E. M., C. R. Homeyer, and J. T. Allen, 2021: A 23-year severe hail climatology using gridrad mesh observations. *Monthly Weather Review*, **149**, 945 – 958, https://doi.org/10.1175/MWR-D-20-0178.1, URL https://journals.ametsoc.org/view/journals/mwre/149/4/MWR-D-20-0178.1.xml.

NCEI, 2023: U.s. billion-dollar weather and climate disasters (2023). URL https://www.ncdc.noaa.gov/billions/.

NCEI/NOAA, 2022: NOAA's Storm Events Database. URL https://www.ncdc.noaa.gov/stormevents/, National Centers for Environmental Information, accessed December 2019 to January 2022.

Accepted for publication in *Monthly Weather Review*. DOI 10.1175/MWR-D-23-0017.1.

NOAA/NWS/ROC, 1991: Noaa next generation radar (nexrad) level ii base data. URL https://doi.org/10.7289/V5W9574V, NOAA National Centers for Environmental Information, accessed December 2019 to January 2022.

Parker, M. D., and R. H. Johnson, 2000: Organizational modes of midlatitude mesoscale convective systems. *Monthly Weather Review*, **128**, 3413 – 3436, https://doi.org/10.1175/1520-0493(2001)129⟨3413:OMOMMC⟩2.0.CO;2, URL https://journals.ametsoc.org/view/journals/mwre/128/10/1520-0493_2001_129_3413_omommc_2.0.co_2.xml.

Pinto, J. O., J. A. Grim, and M. Steiner, 2015: Assessment of the high-resolution rapid refresh model's ability to predict mesoscale convective systems using object-based evaluation. *Weather and Forecasting*, **30**, 892 – 913, https://doi.org/https://doi.org/10.1175/WAF-D-14-00118.1, URL https://journals.ametsoc.org/view/journals/wefo/30/4/waf-d-14-00118_1.xml.

Rockwood, A. A., and R. A. Maddox, 1988: Mesoscale and synoptic scale interactions leading to intense convection: The case of 7 june 1982. *Weather and Forecasting*, **3**, 51 – 68, https://doi.org/https://doi.org/10.1175/1520-0434(1988)003⟨0051:MASSIL⟩2.0.CO;2, URL https://journals.ametsoc.org/view/journals/wefo/3/1/1520-0434_1988_003_0051_massil_2_0_co_2.xml.

Ryzhkov, A., D. Burgess, D. Zrnic, T. Smith, and S. Giangrande, 2002: Polarimetric analyses of a 3 may 1999 tornado. *21st Conf. on Severe Local Storms*, American Meteorological Society, 14.2.

Ryzhkov, A. V., T. J. Schuur, D. W. Burgess, and D. S. Zrnic, 2005: Polarimetric tornado detection. *Journal of Applied Meteorology*, **44**, 557 – 570, https://doi.org/10.1175/JAM2235.1, URL https://journals.ametsoc.org/view/journals/apme/44/5/jam2235.1.xml.

Sandmæl, T. N., 2017: An evaluation of radar- and satellite-data based products to discriminate between tornadic and non-tornadic storms. M.S. thesis, University of Oklahoma, URL https://hdl.handle.net/11244/52775.

Schiesser, H. H., R. A. Houze, and H. Huntrieser, 1995: The mesoscale structure of severe precipitation systems in switzerland. *Monthly Weather Review*, **123**, 2070 – 2097, https://doi.org/10.1175/1520-0493(1995)123⟨2070:TMSOSP⟩2.0.CO;2, URL https://journals.ametsoc.org/view/journals/mwre/123/7/1520-0493_1995_123_2070_tmsosp_2_0_co_2.xml.

Accepted for publication in *Monthly Weather Review*. DOI 10.1175/MWR-D-23-0017.1.

School of Meteorology, University of Oklahoma, 2021: Gridrad-severe - three-dimensional gridded nexrad wsr-88d radar data for severe events. Research Data Archive at the National Center for Atmospheric Research, Computational and Information Systems Laboratory, Boulder CO, URL https://doi.org/10.5065/2B46-1A97.

Schumacher, R. S., and K. L. Rasmussen, 2020: The formation, character and changing nature of mesoscale convective systems. *Nat. Rev. Earth Environ.*, **1**, 300 – 314, URL https://doi.org/10.1038/s43017-020-0057-7.

Smith, B. T., R. L. Thompson, J. S. Grams, C. Broyles, and H. E. Brooks, 2012: Convective modes for significant severe thunderstorms in the contiguous united states. part i: Storm classification and climatology. *Weather and Forecasting*, **27**, 1114 – 1135, https://doi.org/10.1175/WAF-D-11-00115.1, URL https://journals.ametsoc.org/view/journals/wefo/27/5/waf-d-11-00115_1.xml.

Snively, D. V., and W. A. Gallus, 2014: Prediction of convective morphology in near-cloud-permitting wrf model simulations. *Weather and Forecasting*, **29**, 130 – 149, https://doi.org/10.1175/WAF-D-13-00047.1, URL https://journals.ametsoc.org/view/journals/wefo/29/1/waf-d-13-00047_1.xml.

Starzec, M., C. R. Homeyer, and G. L. Mullendore, 2017: Storm labeling in three dimensions (sl3d): A volumetric radar echo and dual-polarization updraft classification algorithm. *Monthly Weather Review*, **145**, 1127 – 1145, https://doi.org/10.1175/MWR-D-16-0089.1, URL https://journals.ametsoc.org/view/journals/mwre/145/3/mwr-d-16-0089.1.xml.

Thielen, J. E., and W. A. Gallus, 2019: Influences of horizontal grid spacing and microphysics on wrf forecasts of convective morphology evolution for nocturnal mcss in weakly forced environments. *Weather and Forecasting*, **34**, 1495 – 1517, https://doi.org/10.1175/WAF-D-18-0210.1, URL https://journals.ametsoc.org/view/journals/wefo/34/5/waf-d-18-0210_1.xml.

Torres, S. M., and C. D. Curtis, 2007: Initial implementation of super-resolution data on the nexrad network. 23rd Conf. on International Interactive Information and Processing Systems (IIPS) for Meteorology, Oceanography, and Hydrology, San Antonio, TX, American Meteorological Society, 5B.10, URL http://ams.confex.com/ams/87ANNUAL/techprogram/paper_116240.htm.

Accepted for publication in *Monthly Weather Review*. DOI 10.1175/MWR-D-23-0017.1.

Trapp, R. J., S. A. Tessendorf, E. S. Godfrey, and H. E. Brooks, 2005: Tornadoes from squall lines and bow echoes. part i: Climatological distribution. *Weather and Forecasting*, **20**, 23 – 34, https://doi.org/10.1175/WAF-835.1, URL https://journals.ametsoc.org/view/journals/wefo/20/1/waf-835_1.xml.

Trapp, R. J., D. M. Wheatley, N. T. Atkins, R. W. Przybylinski, and R. Wolf, 2006: Buyer beware: Some words of caution on the use of severe wind reports in postevent assessment and research. *Weather and Forecasting*, **21**, 408 – 415, https://doi.org/https://doi.org/10.1175/WAF925.1, URL https://journals.ametsoc.org/view/journals/wefo/21/3/waf925_1.xml.

Van Den Broeke, M. S., 2020: A preliminary polarimetric radar comparison of pre-tornadic and nontornadic supercell storms. *Mon. Wea. Rev.*, **148**, 1567–1584, https://doi.org/10.1175/MWR-D-19-0296.1.

Vaughan, M. T., B. H. Tang, and L. F. Bosart, 2017: Climatology and analysis of high-impact, low predictive skill severe weather events in the northeast united states. *Weather and Forecasting*, **32**, 1903 – 1919, https://doi.org/10.1175/WAF-D-17-0044.1, URL https://journals.ametsoc.org/view/journals/wefo/32/5/waf-d-17-0044_1.xml.

Wakimoto, R. M., 2001: *Severe Convective Storms*, chap. Convectively Driven High Wind Events, 255 – 298. Meteorological Monographs, American Meteorological Society, Boston, MA, URL https://doi.org/10.1007/978-1-935704-06-5_7.

Weisman, M. L., and R. J. Trapp, 2003: Low-level mesovortices within squall lines and bow echoes. part i: Overview and dependence on environmental shear. *Monthly Weather Review*, **131**, 2779 – 2803, https://doi.org/https://doi.org/10.1175/1520-0493(2003)131⟨2779:LMWSLA⟩2.0.CO;2, URL https://journals.ametsoc.org/view/journals/mwre/131/11/1520-0493_2003_131_2779_lmwsla_2.0.co_2.xml.

Wendt, N. A., and I. L. Jirak, 2021: An hourly climatology of operational mrms mesh-diagnosed severe and significant hail with comparisons to storm data hail reports. *Weather and Forecasting*, **36**, 645 – 659, https://doi.org/10.1175/WAF-D-20-0158.1, URL https://journals.ametsoc.org/view/journals/wefo/36/2/WAF-D-20-0158.1.xml.

Accepted for publication in *Monthly Weather Review*. DOI 10.1175/MWR-D-23-0017.1.

Wilson, J. W., J. A. Moore, G. B. Foote, B. Martner, A. R. Rodi, T. Uttal, and J. M. Wilczak, 1988: Convection initiation and downburst experiment (cinde). *Bulletin of the American Meteorological Society*, **69**, 1328 – 1347, https://doi.org/10.1175/1520-0477(1988)069⟨1328:CIADE⟩2.0.CO;2, URL https://journals.ametsoc.org/view/journals/bams/69/11/1520-0477_1988_069_1328_ciade_2_0_co_2.xml.

Wilson, J. W., and R. M. Wakimoto, 2001: The discovery of the downburst: T. t. fujita's contribution. *Bulletin of the American Meteorological Society*, **82**, 49 – 62, https://doi.org/10.1175/1520-0477(2001)082⟨0049:TDOTDT⟩2.3.CO;2, URL https://journals.ametsoc.org/view/journals/bams/82/1/1520-0477_2001_082_0049_tdotdt_2_3_co_2.xml.

Witt, A., M. D. Eilts, G. J. Stumpf, J. T. Johnson, E. D. W. Mitchell, and K. W. Thomas, 1998: An enhanced hail detection algorithm for the wsr-88d. *Weather and Forecasting*, **13**, 286 – 303, https://doi.org/10.1175/1520-0434(1998)013⟨0286:AEHDAF⟩2.0.CO;2, URL https://journals.ametsoc.org/view/journals/wefo/13/2/1520-0434_1998_013_0286_aehdaf_2_0_co_2.xml.

Wurman, J., J. M. Straka, and E. N. Rasmussen, 1996: Fine-scale doppler radar observations of tornadoes. *Science*, **272 (5269)**, 1774–1777, https://doi.org/10.1126/science.272.5269.1774, URL https://www.science.org/doi/abs/10.1126/science.272.5269.1774, https://www.science.org/doi/pdf/10.1126/science.272.5269.1774.

Accepted for publication in *Monthly Weather Review*. DOI 10.1175/MWR-D-23-0017.1.